

Cellwise outlier detection in heterogeneous populations

Giorgia Zaccaria*

Department of Statistics and Quantitative Methods, University of Milano-Bicocca
and

Luis A. García-Escudero

Department of Statistics and Operational Research, University of Valladolid
and

Francesca Greselin

Department of Statistics and Quantitative Methods, University of Milano-Bicocca
and

Agustín Mayo-Íscar

Department of Statistics and Operational Research, University of Valladolid

Abstract

Real-world applications may be affected by outlying values. In the model-based clustering literature, several methodologies have been proposed to detect units that deviate from the majority of the data (rowwise outliers) and trim them from the parameter estimates. However, the discarded observations can encompass valuable information in some observed features. Following the more recent cellwise contamination paradigm, we introduce a Gaussian mixture model for cellwise outlier detection. The proposal is estimated via an Expectation-Maximization (EM) algorithm with an additional step for flagging the contaminated *cells* of a data matrix and then imputing – instead of discarding – them before the parameter estimation. This procedure adheres to the spirit of the EM algorithm by treating the contaminated cells as missing values. We analyze the performance of the proposed model in comparison with other existing methodologies through a simulation study with different scenarios and illustrate its potential use for clustering, outlier detection, and imputation on three real data sets. Additional applications include socio-economic studies, environmental analysis, healthcare, and any domain where the aim is to cluster data affected by missing information and outlying values within features.

Keywords: Robustness, Model-based clustering, Cellwise contamination, Missing data, EM algorithm, Imputation

*Corresponding author: giorgia.zaccaria@unimib.it

1 Introduction

Real data often contain outlying and missing values. For instance, health records tracking the presence of a disease could be affected by missing or noisy measurements, while socio-economic surveys about individuals or firms might contain intentionally incorrect responses. In robust statistical literature, several methodologies have been proposed to prevent biased parameter estimates by detecting and downweighting or discarding contaminated cases within a data matrix. These cases typically correspond to entire rows, therefore referred to as rowwise/casewise outliers (Huber, 1964), which are assumed not to follow the distribution of the majority of the data. In recent years, the component-wise contamination model proposed by Alqallaf et al. (2009) has garnered increasing attention from researchers. This introduced a new contamination paradigm that assumes some *cells* of a data matrix have been replaced by arbitrary values. According to it, a low percentage of cellwise contamination potentially corrupts many rows, or even all of them, as the number of variables increases. Consequently, casewise trimming would discard valuable information encompassed in the uncontaminated cells of the rows or be unfeasible. In the single-population framework, the cellwise Minimum Covariance Determinant estimator (cellMCD, Raymaekers and Rousseeuw, 2023) represents the most recent proposal for robustly estimating the location and scale parameters in the presence of cellwise contamination, forerunning by the Detection-Imputation (DI) method (Raymaekers and Rousseeuw, 2021) and other methodologies for several purposes, such as principal component analysis (Hubert et al., 2019; see Raymaekers and Rousseeuw, 2024, for a comprehensive review). Both cellMCD and DI, being based on the Expectation-Maximization (EM) algorithm (Dempster et al., 1977),

can further handle missing values, faithfully adhering to its spirit by treating contaminated cells as missing information to be imputed. However, they assume one single homogeneous population and cannot deal with heterogeneity in the data, which is common in practice.

For uncovering contamination in heterogeneous populations, a first class of models has been proposed which accommodate to the presence of outliers by partially relaxing the normality assumption and considering heavy-tailed distributions for the components. This class encompasses the mixture of t distributions (Peel and McLachlan, 2000) and the mixtures of contaminated normal distributions (Punzo and McNicholas, 2016) as examples, both extended to handle Missing At Random (MAR, Rubin, 1976) values in the data by Wang et al. (2004) and Tong and Tortora (2022), respectively, as is common in other statistical methodologies (Little and Rubin, 2019). To deal with contamination in general position in model-based clustering, García-Escudero et al. (2008) introduced TCLUST, which extended the Minimum Covariance Determinant (MCD, Rousseeuw, 1984, 1985) estimator for the location and covariance matrix through the use of classification trimmed likelihoods. Specifically, TCLUST includes a *Concentration* step (C-step) in the EM algorithm, similar to that in the faster MCD algorithm (FAST-MCD, Rousseeuw and van Driessen, 1999), where a fixed fraction of observations whose contribution to the objective function is the smallest are considered as outliers and discarded from the parameter estimation. An analogous trimming approach was considered in a mixture likelihood model-based framework in Neykov et al. (2007) and García-Escudero et al. (2014).

The goal of this paper is to provide a model-based extension of cellMCD in the clustering framework for coping with cellwise contamination and MAR information. The proposal,

called cellwise Gaussian Mixture Model (cellGMM), is based upon the maximization of the log-likelihood via a mixture EM algorithm with a fixed number of components and including constraints to avoid spurious solutions (García-Escudero et al., 2014). The difficult challenge of simultaneously detecting clustering structures via a model-based approach and identifying outlying cells position, influenced by the variable dependence within sub-populations, has been previously addressed by Farcomeni (2014). His snipping proposal for Gaussian mixture models (sclust) involves the removal of contaminated cells from the E- and M-step of the algorithm. Nonetheless, sclust has some limitations that our proposal seeks to address. Specifically, cellGMM supplies imputation, say “correction”, for outlying values, as well as for missing values whose positions are known. This improves the efficiency of the parameter estimators and eliminates the need for additional correction procedures to avoid undesirable bias (shrinkage) of the component covariance matrices that can occur in discarding approaches. Additionally, cellGMM, unlike sclust, can automatically determine the contamination level in the data matrix while retaining a certain fraction of observations considered non-contaminated per variable. These features enable cellGMM to obtain better results in terms of clustering performance, recovery of outlying cells, and efficiency in parameter estimation, as shown in the simulation study presented in Section 3. It is worth noting that the initialization of cellGMM is a crucial issue, which we will discuss in Section 2.2 and in detail in the Supplementary Material available online. Other approaches for robust clustering based on cellwise trimming can be found in Farcomeni (2013) and García-Escudero et al. (2021). These approaches are no longer be considered in this work because they do not provide estimators of the component covariance matrices and are es-

sentially based on searching for approximating sets made of G points or G affine sub-spaces in the observed data.

The rest of the paper is organized as follows. We describe our proposal in Section 2, along with its computational aspects. Sections 3 and 4 provide evidence of the cellGMM performance compared to other existing methodologies for casewise and cellwise outlier detection through a simulation study and three real-world applications involving spectral data, image reconstruction and data on cars' features. Finally, a discussion reviews the obtained results and presents open research lines for future investigation in Section 5.

2 Gaussian mixture models with cellwise outliers

The proposed methodology follows in the footsteps of cellMCD by leveraging the EM algorithm in the model-based clustering framework. Consider a p -dimensional random vector drawn from a mixture of G multivariate Gaussian distributions, whose probability density function (pdf) is given by

$$f(\mathbf{x}; \boldsymbol{\Psi}) = \sum_{g=1}^G \pi_g \phi_p(\mathbf{x}; \boldsymbol{\mu}_g, \boldsymbol{\Sigma}_g), \quad (1)$$

where $\phi_p(\cdot; \boldsymbol{\mu}, \boldsymbol{\Sigma})$ is the pdf of the p -variate normal with mean $\boldsymbol{\mu}$ and covariance matrix $\boldsymbol{\Sigma}$. $\boldsymbol{\Psi} = \{\boldsymbol{\pi}, \boldsymbol{\theta}\}$ is the overall parameter set composed of $\boldsymbol{\pi} = \{\pi_g\}_{g=1}^G$ with weights $\pi_g \in (0, 1]$ and such that $\sum_{g=1}^G \pi_g = 1$, and $\boldsymbol{\theta} = \{\boldsymbol{\mu}_g, \boldsymbol{\Sigma}_g\}_{g=1}^G$ with component mean vectors $\boldsymbol{\mu}_g \in \mathbb{R}^p$ and symmetric positive definite component covariance matrices $\boldsymbol{\Sigma}_g \in \mathbb{R}^{p \times p}$.

Let $\mathbf{X} = [x_{ij} : i = 1, \dots, n, j = 1, \dots, p]$ be a data matrix, whose rows $\mathbf{x}_1, \dots, \mathbf{x}_n$, with $\mathbf{x}_i \in \mathbb{R}^p$, are supposed to be a random sample drawn from GMM in (1). It can

happen that some individual measurements or cells, i.e., some x_{ij} , have been replaced by outlying values. We refer to the latter as *contaminated* or *unreliable* cells, that can be distributed everywhere throughout the sample. To track their pattern, we define the matrix $\mathbf{W} = [w_{ij} : i = 1, \dots, n, j = 1, \dots, p]$, where $w_{ij} = 1$ if x_{ij} is reliable, and $w_{ij} = 0$ if not because it has been contaminated. We use herein the notation $\mathbf{w}_i, i = 1, \dots, n$, when referring to the rows of \mathbf{W} , but we denote with $\mathbf{W}_{\cdot j}$ the j th column of that matrix (equivalent notation will be used for other matrices considered in this work). According to the values of \mathbf{w}_i , we partition \mathbf{x}_i into $\mathbf{x}_{i[\mathbf{w}_i]}$ and $\mathbf{x}_{i[\mathbf{1}_p - \mathbf{w}_i]}$ (respectively, reliable and unreliable cells in the observation \mathbf{x}_i), where $\mathbf{1}_p$ is a p -dimensional unitary vector. Henceforth, we refer to $\mathbf{1}_p - \mathbf{w}_i$ as \mathbf{w}_i^c for simplicity. In a similar manner, given a vector $\boldsymbol{\mu} \in \mathbb{R}^p$, $\boldsymbol{\mu}_{[\mathbf{w}_i]}$ stands for its sub-vector in $\mathbb{R}^{p[\mathbf{w}_i]}$, where $p[\mathbf{w}_i] = \sum_{j=1}^p w_{ij}$, i.e., the sub-vector corresponding to the cells of \mathbf{x}_i for which $w_{ij} = 1$. Analogously, $\boldsymbol{\Sigma}_{[\mathbf{w}_i, \mathbf{w}_i]}$ symbolizes the $p[\mathbf{w}_i] \times p[\mathbf{w}_i]$ sub-matrix of $\boldsymbol{\Sigma} \in \mathbb{R}^{p \times p}$ obtained by keeping only the rows and columns of $\boldsymbol{\Sigma}$ whose indexes j satisfy $w_{ij} = 1$ in \mathbf{w}_i . Finally, with $\boldsymbol{\mu}_{[j]} (\boldsymbol{\Sigma}_{[j,j]})$ we extract the j th (jj th) element of $\boldsymbol{\mu}$ ($\boldsymbol{\Sigma}$).

Considering the notation introduced, the objective function of the Gaussian Mixture Model with cellwise outliers (cellGMM) to maximize is

$$\ell(\boldsymbol{\Psi}, \mathbf{W}; \mathbf{X}) = \sum_{i=1}^n \ln \left[\sum_{g=1}^G \pi_g \phi_{p[\mathbf{w}_i]}(\mathbf{x}_{i[\mathbf{w}_i]}; \boldsymbol{\mu}_{g[\mathbf{w}_i]}, \boldsymbol{\Sigma}_{g[\mathbf{w}_i, \mathbf{w}_i]}) \right], \quad (2)$$

subject to constraints

$$\|\mathbf{W}_{\cdot j}\|_0 \geq h, \forall j = 1, \dots, p, \quad (3)$$

$$\frac{\max_{g=1, \dots, G} \max_{j=1, \dots, p} \lambda_j(\boldsymbol{\Sigma}_g)}{\min_{g=1, \dots, G} \min_{j=1, \dots, p} \lambda_j(\boldsymbol{\Sigma}_g)} \leq c, \quad (4)$$

where $\lambda_j(\boldsymbol{\Sigma}_g)$ is the j th eigenvalue of the covariance matrix $\boldsymbol{\Sigma}_g$ and $c \geq 1$ is a fixed constant

(García-Escudero et al., 2008). The constraint in (3) requires at least h reliable cells in each column, so we set $h \geq 0.75n$ (see Raymaekers and Rousseeuw, 2023). The eigenvalue-ratio constraint in (4) addresses the problem of the unboundedness of (2) and the spurious solutions that may result from its maximization, while maintaining the positive definiteness of Σ_g .

To solve the constrained maximization in (2), we consider an adaptation of the EM algorithm – typically used for mixture modeling and handling of missingness in the data – which allows to simultaneously detect the outlying cells and find the maximum likelihood estimates of the model parameters. In this EM framework, there are multiple sources of unknown information beyond the model parameters: firstly, the outlying cells of $\{\mathbf{x}_i\}_{i=1}^n$ corresponding to the zeros in $\{\mathbf{w}_i\}_{i=1}^n$, and, secondly, the indicator to the population belonging, also called unit-component membership, reported in $\mathbf{Z} = [z_{ig} : i = 1, \dots, n, g = 1, \dots, G]$, where $z_{ig} = 1$ if the i th observation belongs to the g th component of the mixture, and $z_{ig} = 0$ otherwise. Let \mathbf{z}_i and $\mathbf{x}_{i[\mathbf{w}_i^c]}$ be the “missing” data, and $\mathbf{x}_{i[\mathbf{w}_i]}$ the observed data. The cellGMM complete data log-likelihood is

$$\ell_c(\boldsymbol{\Psi}, \mathbf{W}, \mathbf{Z}; \mathbf{X}) = \sum_{i=1}^n \sum_{g=1}^G z_{ig} \left[\ln(\pi_g) + \ln(\phi_p(\mathbf{x}_{i[\mathbf{w}_i]}, \mathbf{x}_{i[\mathbf{w}_i^c]}; \boldsymbol{\mu}_g, \Sigma_g)) \right] \quad (5)$$

subject to constraints (3) and (4). In the following, we detail the steps of the EM algorithm for the estimation of the cellGMM parameters. The algorithm starts with initial solutions for the parameters, which will be discussed in Section 2.2. The C-step involves estimating \mathbf{W} , whereas the E-step consists of computing expectations of the remaining missing data. In the M-step, we derive the estimates of the overall parameter set $\boldsymbol{\Psi}$.

Update of \mathbf{W} . At iteration $(t+1)$, given $\widehat{\boldsymbol{\Psi}}^{(t)}$ and $\mathbf{Z}^{(t)}$, we update the configuration of

\mathbf{W} column-by-column. To simplify the notation, we use an intermediate $\widetilde{\mathbf{W}}$ matrix before providing the updated $\mathbf{W}^{(t+1)}$. Consequently, we start from $\widetilde{\mathbf{W}} = \mathbf{W}^{(t)}$ and we update $\widetilde{\mathbf{W}}_{\cdot j}$ sequentially for $j = 1, \dots, p$, by considering the previously estimated $(j - 1)$ columns of $\widetilde{\mathbf{W}}$ as fixed. To this aim, we define the contribution of the i th observation to the cellGMM objective function in (2) as

$$\ell_{(i)}(\boldsymbol{\Psi}, \mathbf{w}_i; \mathbf{x}_i) = \ln \left[\sum_{g=1}^G \pi_g \phi_{p[\mathbf{w}_i]}(\mathbf{x}_{i[\mathbf{w}_i]}; \boldsymbol{\mu}_{g[\mathbf{w}_i]}, \boldsymbol{\Sigma}_{g[\mathbf{w}_i, \mathbf{w}_i]}) \right]. \quad (6)$$

For the j th column of $\widetilde{\mathbf{W}}$, we compare the contribution of the i th unit to the observed log-likelihood in (6) when we modify the j th element of $\widetilde{\mathbf{w}}_i$ such that its value for the i th observation is considered reliable ($w_{ij} = 1$) or contaminated ($w_{ij} = 0$), while the other terms in $\widetilde{\mathbf{w}}_i$ remain unchanged. Therefore, we compute

$$\Delta_{ij} = \ell_{(i)}(\widehat{\boldsymbol{\Psi}}^{(t)}, \widetilde{\mathbf{w}}_i; \mathbf{x}_i, \widetilde{w}_{ij} = 1) - \ell_{(i)}(\widehat{\boldsymbol{\Psi}}^{(t)}, \widetilde{\mathbf{w}}_i; \mathbf{x}_i, \widetilde{w}_{ij} = 0). \quad (7)$$

With the aim of maximizing the observed log-likelihood $\sum_{i=1}^n \ell_{(i)}(\widehat{\boldsymbol{\Psi}}^{(t)}, \mathbf{w}_i; \mathbf{x}_i)$ subject to constraint (3), we attain the optimum by setting $\widetilde{w}_{ij} = 1$ for all indexes i corresponding to the h largest values of $\{\Delta_{ij}\}_{i=1}^n$, 0 otherwise. Repeating this procedure for all columns of $\widetilde{\mathbf{W}}$ we obtain $\mathbf{W}^{(t+1)} = \widetilde{\mathbf{W}}$. As shown in Raymaekers and Rousseeuw (2023), the chosen order for the update of \mathbf{W} does not seem to significantly affect the performance of the procedure. It is worth noting that the rationale for updating \mathbf{W} is inspired by the approach proposed in Raymaekers and Rousseeuw (2023). Nevertheless, it is tailored to a Gaussian mixture model framework.

Update of \mathbf{Z} and $\mathbf{X}_{[\mathbf{w}^c]}$. At iteration $(t + 1)$, we update the membership matrix \mathbf{Z} and the unreliable data in \mathbf{X} corresponding to the zero elements into $\mathbf{W}^{(t+1)}$. For this

purpose, we consider the outlying cells uncovered in $\mathbf{W}^{(t+1)}$ as missing values. We compute the expected value of the complete data log-likelihood in (5) conditional on the observed and reliable data, given $\mathbf{W}^{(t+1)}$ and the current estimate of the parameter set in $\widehat{\boldsymbol{\Psi}}^{(t)}$, i.e. $\mathbb{E}[\ell_c(\boldsymbol{\Psi}, \mathbf{W}^{(t+1)}, \mathbf{Z}; \mathbf{X})|\mathbf{X}_{[\mathbf{W}^{(t+1)}]}; \widehat{\boldsymbol{\Psi}}^{(t)}]$, as follows

$$Q(\boldsymbol{\Psi}; \widehat{\boldsymbol{\Psi}}^{(t)}) = \sum_{i=1}^n \sum_{g=1}^G \mathbb{E}[Z_{ig}|\mathbf{x}_{i[\mathbf{w}_i^{(t+1)}]}; \widehat{\boldsymbol{\Psi}}^{(t)}] \times \left\{ \ln(\pi_g) - \frac{1}{2} \left[\ln(|\boldsymbol{\Sigma}_g|) + \text{tr}(\boldsymbol{\Sigma}_g^{-1} \right. \right. \\ \left. \left. \mathbb{E}[(\mathbf{x}'_{i[\mathbf{w}_i^{(t+1)}]}, \mathbf{X}'_{i[\mathbf{w}_i^{(t+1)c}]})' - \boldsymbol{\mu}_g] (\mathbf{x}'_{i[\mathbf{w}_i^{(t+1)}]}, \mathbf{X}'_{i[\mathbf{w}_i^{(t+1)c}]})' - \boldsymbol{\mu}_g)' | \mathbf{x}_{i[\mathbf{w}_i^{(t+1)}]}, z_{ig} = 1; \widehat{\boldsymbol{\Psi}}^{(t)}] \right) \right\}, \quad (8)$$

where we omit the constant term of the normal distribution not depending on the model parameters. The computation of all the conditional expectations required in (8), which correspond to those presented by Ghahramani and Jordan (1995) for GMM with missing data, is reported in Section 1.1 of the Supplementary Material. These expectations constitute the E-step of the proposed algorithm, while the M-step maximizes $Q(\boldsymbol{\Psi}; \widehat{\boldsymbol{\Psi}}^{(t)})$ with respect to $\boldsymbol{\Psi}$ by updating the estimates of the cellGMM parameters. The latter correspond to the usual estimates of the GMM parameters computed on the *completed* data $\left\{ \left\{ \tilde{\mathbf{x}}_{i(g)}^{(t+1)} = (\mathbf{x}_{i[\mathbf{w}_i^{(t+1)}]}, \widehat{\mathbf{x}}_{i[\mathbf{w}_i^{(t+1)c}]^{(g)}})' \right\}_{g=1}^G \right\}_{i=1}^n$ (see Section 1.1 of the Supplementary Material for details).

2.1 Penalized log-likelihood approach for cellGMM

The EM algorithm described for estimating the cellGMM parameters uncovers a fixed number h of hopefully reliable cells per variable through \mathbf{W} . However, the cellwise outlier contamination can affect the variables differently. To prevent excessive cell flagging, we

add penalty terms to the log-likelihood in (2) as follows

$$\ell_{\text{pen}}(\boldsymbol{\Psi}, \mathbf{W}; \mathbf{X}) = \sum_{i=1}^n \ln \left[\sum_{g=1}^G \pi_g \phi_{p[\mathbf{w}_i]}(\mathbf{x}_{i[\mathbf{w}_i]}; \boldsymbol{\mu}_{g[\mathbf{w}_i]}, \boldsymbol{\Sigma}_{g[\mathbf{w}_i, \mathbf{w}_i]}) \right] - \sum_{j=1}^p \sum_{i=1}^n q_{ij}(1 - w_{ij}), \quad (9)$$

where $\mathbf{Q} = [q_{ij} : i = 1, \dots, n, j = 1, \dots, p]$ represents a tuning matrix (see Section 2.2 for the details on its setting). Maximizing (9) under constraints (3) and (4) can avoid detecting an unnecessary high number of contaminated cells for an appropriate \mathbf{Q} matrix. It is worth noting that the penalty term plays a crucial role in the update of \mathbf{W} , while it can be ignored in the other steps of the cellGMM algorithm. Specifically, the penalized version of the C-step is described below.

Penalized update of \mathbf{W} . Inspired by the rationale in Raymaekers and Rousseeuw (2023), we propose a modified Δ_{ij} , denoted as $\tilde{\Delta}_{ij}$, which is defined from

$$\tilde{\ell}_{(i)}(\boldsymbol{\Psi}, \mathbf{w}_i, \mathbf{z}_i; \mathbf{x}_i) = \sum_{g=1}^G z_{ig} \left[\ln(\pi_g) + \ln(\phi_{p[\mathbf{w}_i]}(\mathbf{x}_{i[\mathbf{w}_i]}; \boldsymbol{\mu}_{g[\mathbf{w}_i]}, \boldsymbol{\Sigma}_{g[\mathbf{w}_i, \mathbf{w}_i]})) \right] - \sum_{j=1}^p q_{ij}(1 - w_{ij}), \quad (10)$$

as

$$\begin{aligned} \tilde{\Delta}_{ij} &= \tilde{\ell}_{(i)}(\hat{\boldsymbol{\Psi}}^{(t)}, \tilde{\mathbf{w}}_i, \mathbf{z}_i^{(t)}; \mathbf{x}_i, \tilde{w}_{ij} = 1) - \tilde{\ell}_{(i)}(\hat{\boldsymbol{\Psi}}^{(t)}, \tilde{\mathbf{w}}_i, \mathbf{z}_i^{(t)}; \mathbf{x}_i, \tilde{w}_{ij} = 0) \\ &= -\frac{1}{2} \left\{ \sum_{g=1}^G z_{ig}^{(t)} \left[\ln(\hat{C}_{ij(g)}) + \frac{(x_{ij} - \hat{x}_{ij(g)})^2}{\hat{C}_{ij(g)}} \right] + \ln(2\pi) \right\} + q_{ij}, \end{aligned} \quad (11)$$

where $\hat{x}_{ij(g)} = \hat{\boldsymbol{\mu}}_{g[j]}^{(t)} + \hat{\boldsymbol{\Sigma}}_{g[j, \tilde{\mathbf{w}}_i]}^{(t)} (\hat{\boldsymbol{\Sigma}}_{g[\tilde{\mathbf{w}}_i, \tilde{\mathbf{w}}_i]}^{(t)})^{-1} (\mathbf{x}_{i[\tilde{\mathbf{w}}_i]} - \hat{\boldsymbol{\mu}}_{g[\tilde{\mathbf{w}}_i]}^{(t)})$ and $\hat{C}_{ij(g)} = \hat{\boldsymbol{\Sigma}}_{g[j, j]}^{(t)} - \hat{\boldsymbol{\Sigma}}_{g[j, \tilde{\mathbf{w}}_i]}^{(t)} (\hat{\boldsymbol{\Sigma}}_{g[\tilde{\mathbf{w}}_i, \tilde{\mathbf{w}}_i]}^{(t)})^{-1} \hat{\boldsymbol{\Sigma}}_{g[\tilde{\mathbf{w}}_i, j]}^{(t)}$ are the expectation and the variance, respectively, of the cell X_{ij} for

the g th mixture component conditional on the reliable cells in the same row i , excluding the j th variable. We obtain this result thanks to the additive property of the Mahalanobis distance and log-likelihood reported in Raymaekers and Rousseeuw (2023, Proposition 5), which stem from the Gaussian distribution properties.

In this case, the update of $\widetilde{\mathbf{W}}_{\cdot j}$, and precisely the number of cells flagged as outliers, depends on the values of $\widetilde{\Delta}_{ij}$: a) if the number of nonnegative $\widetilde{\Delta}_{ij}$ is *greater than* h , i.e., $\#\{\widetilde{\Delta}_{ij} \geq 0\} > h$, we set to one the corresponding cells \widetilde{w}_{ij} for which $\widetilde{\Delta}_{ij} \geq 0$, and to zero the others; b) if the number of nonnegative $\widetilde{\Delta}_{ij}$ is *lower than or equal to* h , i.e., $\#\{\widetilde{\Delta}_{ij} \geq 0\} \leq h$, we set to one the cells \widetilde{w}_{ij} corresponding to the h highest $\widetilde{\Delta}_{ij}$, and to zero the other cells. Consequently, a higher number of cells can be considered as reliable in scenario a), whereas this number is h in scenario b). The penalized log-likelihood approach aims to enable the cellGMM algorithm to recover cells *wrongly* flagged by the unpenalized cellGMM, potentially improving estimation accuracy, as we will see in Section 3.

2.2 Computational issues

Initialization. In the implementation of the EM-type algorithm for estimating the cell-GMM parameters, their initialization is pivotal. In Section 1.2 of the Supplementary Material, we detail the procedure proposed to obtain initial solutions for \mathbf{W} and Ψ , along with the tuning parameters' setting used in our experiments. The initialization involves applying TCLUST individually to each variable and pairs of variables with a fixed trimming level for the initial solution of \mathbf{W} and computing TCLUST on random subsets of variables, followed by a trimmed k -means (Cuesta-Albertos et al., 1997) type algorithm to obtain the initial solution for Ψ . The provided procedure has proved to be compelling aligning closely with the rationale underlying cellGMM. Nonetheless, alternative approaches could be implemented to tackle this issue, that remains open for future work.

Missing information. The cellGMM algorithm can be applied to data with missing

information. Specifically, the cells of \mathbf{W} corresponding to the missing values in \mathbf{X} are set to 0, and the update of \mathbf{W} is computed only on the observed cells.

Stopping criterion and monotonicity. The stopping criterion adopted in the cellGMM algorithm is the Aitken acceleration procedure (Böhning et al. 1994; McLachlan and Peel 2000, Section 2.11; McLachlan and Krishnan 2008, Section 4.9). Moreover, the cellGMM algorithm is monotone, as the objective function is non-decreasing in every iteration. Further details on these aspects are provided in Section 1.3 of the Supplementary Material.

Setting of the penalization tuning matrix \mathbf{Q} . Following Raymaekers and Rousseeuw (2023), we set the generic element of \mathbf{Q} as

$$q_{ij} = \frac{1}{2} \left[\sum_{g=1}^G \hat{z}_{ig} \ln \left(\frac{1}{(\hat{\Sigma}_g^{-1})_{[j,j]}} \right) + \chi_{1,1-\alpha}^2 + \ln(2\pi) \right], \quad (12)$$

where \hat{z}_{ig} and $\hat{\Sigma}_g$ are the estimates obtained at convergence by cellGMM with no penalty (i.e., $\mathbf{Q} = \mathbf{0}$), and $\chi_{1,1-\alpha}^2$ is the quantile of the chi-squared distribution with one degree of freedom and probability $1 - \alpha$ ($\alpha = 0.01$ in our experiments). As we will show in Section 3, the use of the penalized log-likelihood approach for cellGMM usually increases its effectiveness.

3 Simulation study

We carry out herein a simulation study to assess the performance of cellGMM in clustering and parameter estimation recovery. We generate random samples from (1) by considering three scenarios: *Scenario 1* and *Scenario 2* with $n = 200, p = 5, G = 2$, non-spherical with $\Sigma_1 = \Sigma_2 = [\sigma_{ij} = 0.9^{|i-j|} : i, j = 1, \dots, p]$, unbalanced ($\pi = [0.3, 0.7]$), and well-

separated and close components, respectively; *Scenario 3* with $n = 400, p = 15, G = 4$, non-spherical (like Scenarios 1 and 2 with 4 components), unbalanced ($\boldsymbol{\pi} = [0.2, 0.2, 0.3, 0.3]$), and well-separated components. The component mean vectors are generated from uniform distributions. Specifically, $\boldsymbol{\mu}_1 = \mathbf{0}$, and the elements of $\boldsymbol{\mu}_g, g = 2, \dots, G$, are drawn from a uniform distribution in $[0, 10]$ in the well-separated case, and from $[1, 3]$ in the close case. In the former, we assess whether the distance between the component mean vectors is less than 5, and re-generate them if this occurs. The components' configuration is controlled through the overlapping measure ω introduced by Maitra and Melnykov (2010), where well-separated and close components correspond to $\omega_{\max} < 0.01$ and $0.05 < \omega_{\max} < 0.06$, respectively. For each scenario, we obtain 100 data matrices that we contaminate with 0%, 5%, and 10% of outlying cells randomly drawn from a uniform distribution in the interval $[-10, 10]$, ensuring that the contaminated observations do not lie within the 99th percentile ellipsoid of any component. Therefore, we consider 900 random samples altogether. Additional scenarios with missing data, more extreme contamination, and structural outliers are reported in the Supplementary Material.

First, we apply cellGMM without any penalty (cellGMM.pen0). Afterward, we run the penalized version of the algorithm (cellGMM.penb) with the same initialization, using the penalty defined in (12), which is derived from the parameters estimated at the convergence of the unpenalized cellGMM. The proposed methodology is also compared with those illustrated in Section 1: i) TCLUST (R package `tclust`) with 25% of contamination, where we determine the membership of the trimmed units, which are not assigned to any cluster, by computing their posterior probabilities using the parameters estimated by

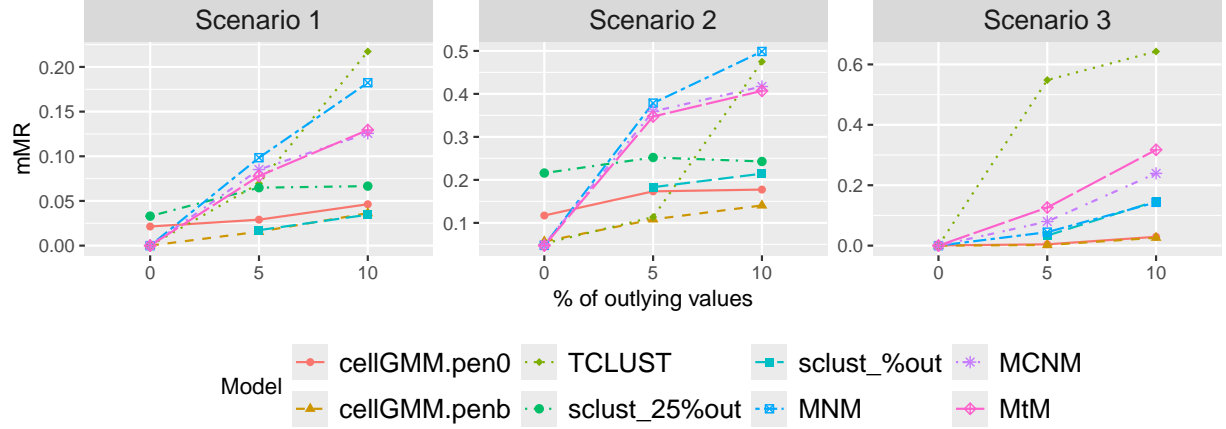


Figure 1: Results of the simulation study: mean of the Misclassification Rate (mMR) per scenario, percentage of contamination, and model

TCLUST at convergence; ii) sclusl (R package `snipEM`) with the suggested initialization for \mathbf{W} by considering 25% and the true percentage of outliers per variable; iii-v) Multivariate Normal Mixture (MNM), Multivariate Contaminated Normal Mixture (MCNM) and Multivariate t Mixture with 25% of contamination (MtM), which are implemented in the R package `MixtureMissing`. The classification performance of the models is evaluated through the Misclassification Rate, while the recovery of the parameters is assessed via the Mean Squared Error for the component mean vectors and the Kullback-Leibler discrepancy for the component covariance matrices (see the Supplementary Material for additional evaluation indices). To correctly compute the latter, we need to solve the label switching problem. With this aim, we order the estimated components via the complete likelihood-based labelling method introduced by Yao (2015). The results reported in Figures 1 and 2 show that the penalized version of cellGMM usually outperforms the unpenalized one, especially when the number of variables is higher and the components are well-separated

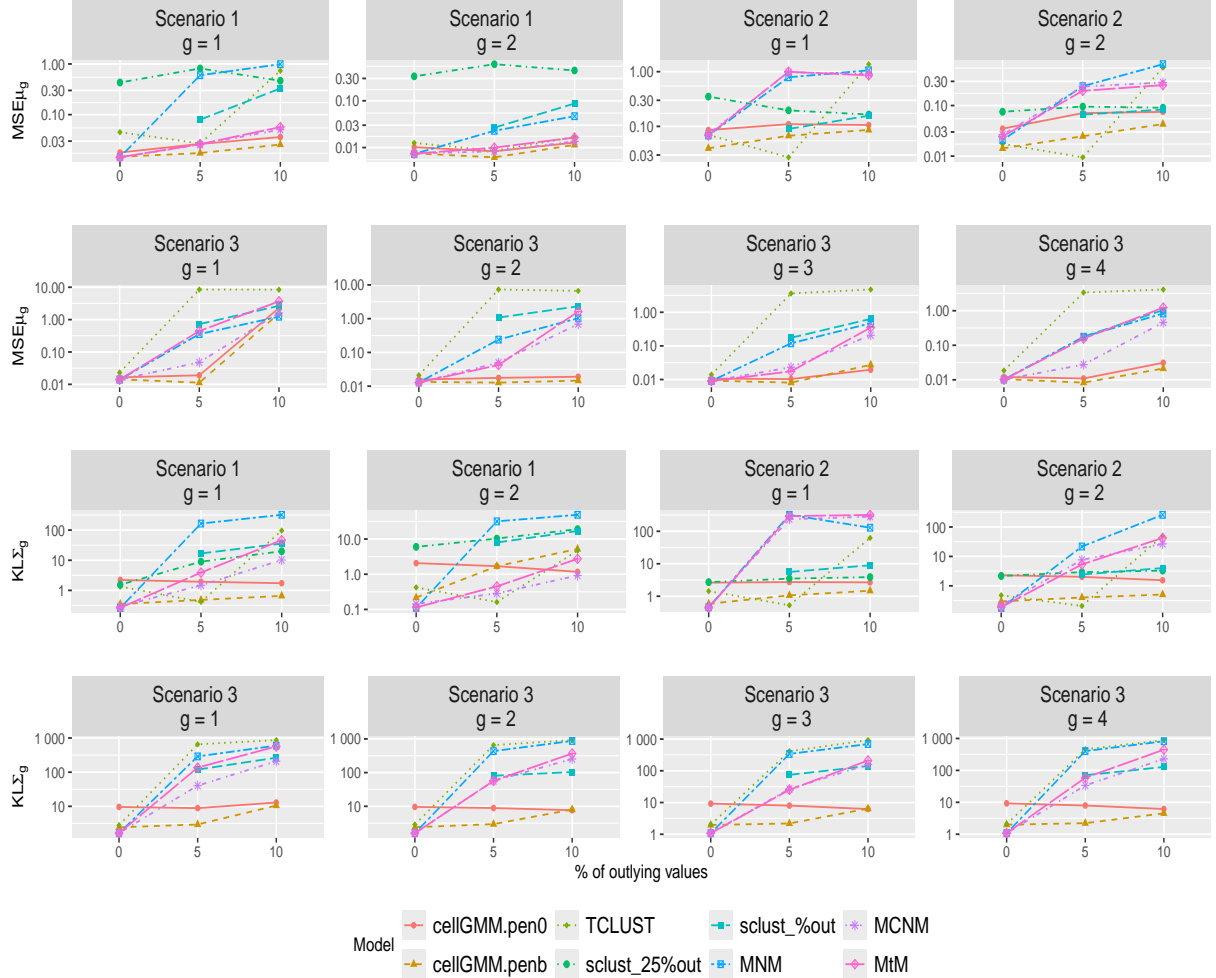


Figure 2: Results of the simulation study: Mean Squared Error (MSE) of the component mean vectors and Kullback-Leibler (KL) discrepancy for the component covariance matrices per scenario, percentage of contamination, and model. The values are represented via log-transformation, while the y-axis ticks are labeled using the original scale

(Scenario 3). In this case, cellGMM benefits from the relationships among variables in the imputation of the outlying cells, which in turn affects the parameter estimates, unlike `sclust` which trims them out. Additionally, the higher the contamination level, the greater the difference between `cellGMM.penb` and the methodologies for rowwise outlier detection, i.e., `TCLUST`, `MCNM` and `MtM`, or the non-robust GMM, i.e. `MNM`. This is due to the fact that cellwise outliers spread out through the observations as the contamination level increases. Therefore, they can affect more than half of the rows, leading to severely biased parameter estimates, even for methods like `TCLUST` (see the results for 10% of contamination in Figure 2).

To address the correct detection of outliers and data matrix imputation, we compute the percentage of True and False Positives on one hand, and the Mean Absolute Error and Root Mean Squared Error between the original and imputed data matrices on the other hand. To this aim, we also consider `cellMCD` and `DI` from the R package `cellWise`. For the model-based clustering methodologies with rowwise outlier detection, we build a \mathbf{W} matrix by setting to zero all the cells of the rows that have been flagged as contaminated. Table 1 illustrates the results. In this case as well, the penalized version of `cellGMM` outperforms the unpenalized one in detecting the unreliable cells, with a drastic decrease in the percentage of false positives and a slight decrease in the true positive due to the enlarged number of cells flagged in `cellGMM.pen0` by constraint. The accurate identification of outliers is reflected in enhanced values for the indices assessing the imputation of contaminated cells, with improvements between `cellGMM.pen0` and `cellGMM.penb`. Due to this better performance, we report the results of `cellGMM.penb` directly in Section 4.

Table 1: Outlier detection and imputation: percentage of True and False Positive (%TP and %FP), Mean Absolute and Root Mean Squared Error (MAE and RMSE) for comparing the original and imputed data matrices per scenario, percentage of contamination, and model

		Scenario 1				Scenario 2				Scenario 3			
% out.	Method	%TP	%FP	MAE	RMSE	%TP	%FP	MAE	RMSE	%TP	%FP	MAE	RMSE
0	cellGMM.pen0	-	25.00	0.22	0.55	-	25.00	0.21	0.46	-	25.00	0.20	0.44
	cellGMM.penb	-	2.26	0.02	0.15	-	3.31	0.04	0.20	-	2.78	0.03	0.16
	TCLUST	-	25.00	-	-	-	25.00	-	-	-	25.00	-	-
	sclust_25	-	25.00	-	-	-	25.00	-	-	-	-	-	-
	MCNM	-	6.38	-	-	-	4.57	-	-	-	40.69	-	-
	MtM	-	26.05	-	-	-	25.14	-	-	-	25.12	-	-
	cellMCD	-	13.76	0.51	1.47	-	2.17	0.02	0.18	-	5.52	0.30	1.39
	DI	-	12.66	0.46	1.36	-	1.93	0.02	0.19	-	15.24	0.68	1.91
5	cellGMM.pen0	96.20	21.25	0.24	0.68	97.30	21.19	0.22	0.51	96.64	21.23	0.22	0.56
	cellGMM.penb	96.56	3.56	0.10	0.56	96.80	5.37	0.10	0.40	95.47	3.78	0.06	0.29
	TCLUST	99.56	21.08	-	-	99.66	21.07	-	-	54.65	23.44	-	-
	sclust_25	71.61	22.55	-	-	92.36	21.45	-	-	-	-	-	-
	sclust_5	54.67	2.39	-	-	77.71	1.17	-	-	45.64	2.86	-	-
	MCNM	93.58	17.29	-	-	57.02	10.28	-	-	75.33	35.55	-	-
	MtM	99.54	36.48	-	-	59.86	32.31	-	-	92.51	48.36	-	-
	cellMCD	94.20	13.71	0.53	1.49	96.76	2.20	0.05	0.23	92.18	3.87	0.22	1.10
10	DI	92.12	5.29	0.19	0.64	96.78	1.97	0.05	0.24	90.03	12.37	0.57	1.68
	cellGMM.pen0	94.98	17.22	0.29	0.89	95.47	17.17	0.22	0.55	93.47	17.39	0.29	0.84
	cellGMM.penb	94.31	6.31	0.20	0.84	94.87	6.33	0.15	0.52	92.01	6.13	0.17	0.68
	TCLUST	64.94	20.56	-	-	65.35	20.52	-	-	44.14	22.87	-	-
	sclust_25	70.30	19.97	-	-	89.45	17.84	-	-	-	-	-	-
	sclust_10	59.12	4.54	-	-	78.97	2.34	-	-	48.88	5.68	-	-
	MCNM	92.77	31.86	-	-	50.94	16.14	-	-	70.27	45.49	-	-
	MtM	96.21	40.92	-	-	60.56	34.19	-	-	77.39	52.65	-	-
	cellMCD	89.46	13.32	0.68	1.82	94.62	2.07	0.07	0.28	88.55	3.28	0.21	1.00
	DI	89.45	2.53	0.12	0.49	94.67	1.92	0.07	0.28	88.56	5.68	0.28	1.06

In Table 1, the difference between the proposal and the model-based clustering methodologies sharpens as the contamination level increases and components overlap, up to the higher-dimensional case (Scenario 3), where cellGMM generally outperforms the competitors significantly. The single-population methods have better results in Scenario 2 with close components, as expected, since it is more likely that the components are so overlapping that they appear as a single population. In contrast, their performance unsurprisingly worsens in Scenario 1 and Scenario 3, both in terms of %TP and %FP. However, it is worth noting that in Scenario 1 with 10% of contamination, DI has lower %FP and imputation indices than cellGMM, despite having a lower %TP. This is riskier for a robust model since the failure to detect outliers can heavily affect the parameter estimates. The peculiar behavior of cellGMM compared to DI in Scenario 1 with 10% of contamination, especially in the imputation results, is due to a higher misclassification rate of the former, which can favor DI over cellGMM. Indeed, if the components are well-separated and a unit is misclassified, the imputation within the wrong component is worse than the DI's imputation between the two components. The additional scenarios illustrated in the Supplementary Material provide further insights into the performance of cellGMM and its competitors.

4 Real data examples

4.1 Homogenized Meat Data Set

In this section, we analyze the homogenized meat data set presented by McElhinney et al. (1999) to evaluate the cellGMM performance in correctly classifying the samples from their visible and infrared spectra. For each of the 231 homogenized meat samples, we consider

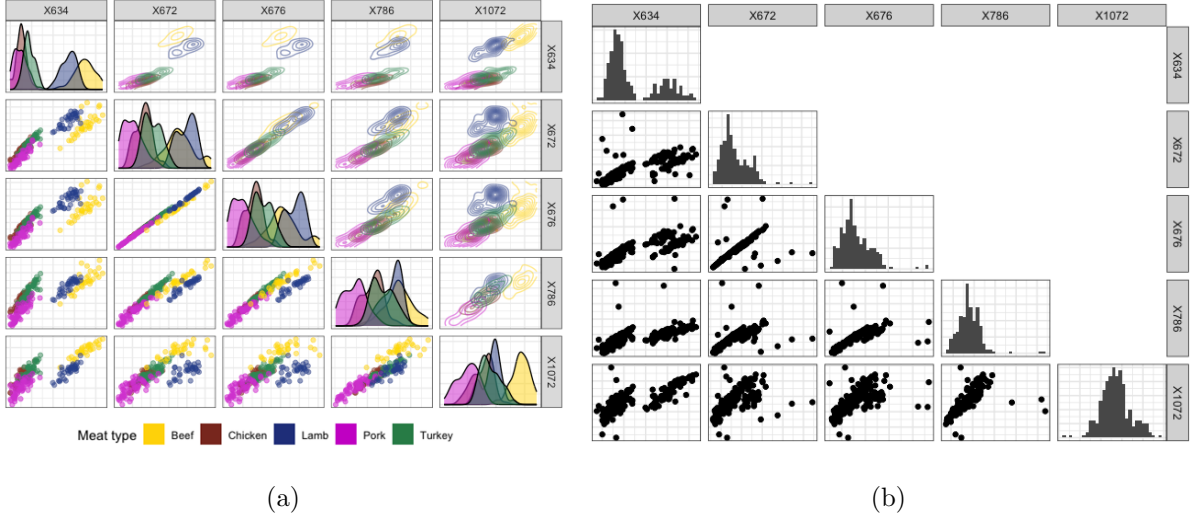


Figure 3: Homogenized Meat data set. (a) Pair plot of 5 variables from the original data: true classification in five homogenized meat types; (b) Pair plot of the data with 3% of cellwise contamination

the five relevant wavelengths which span the protein spectral region (Cappozzo et al., 2021): the first four belonging to the visible part of the spectrum (634 nm, 672 nm, 676 nm and 786 nm) and the remaining one within the near-infrared part (1072 nm). It is worth noting that, even if the original classes are five (beef, chicken, lamb, pork, turkey), some of the selected variables, such as the wavelengths 634 nm and 676 nm, turn out to be important to distinguish red meats (beef and lamb) from white meats (chicken, pork and turkey). This evidence was also highlighted by Murphy et al. (2010) and can be seen in Figure 3a as well. Therefore, we consider the classification of samples in two classes and randomly adulterate them via 3% (without and with 2% of missing) and 10% of cellwise contamination in the range [0.73, 1.25] (see Figure 3b as an example).

We run cellGMM, TCLUST, MNM, MCNM, and MtM with the same settings used

Table 2: Misclassification rate comparing the theoretical and the estimated classification of meat samples in two classes per model and percentage of contamination and missing values, i.e. $(a\%, b\%)$

	cellGMM	TCLUST	sclust	MNM	MCNM	MtM
(0%, 0%)	0.01	0.00	0.00	0.00	0.00	0.00
(3%, 0%)	0.01	0.03	0.04	0.05	0.05	0.06
(3%, 2%)	0.01	-	-	0.05	0.06	0.06
(10%, 0%)	0.02	0.16	0.07	0.15	0.25	0.20

in the simulation study. For sclust, we use the theoretical level of contamination, except when no missing data or outliers are introduced; in such case, the trimming (snipping) level is set to 0.01. As reported in Table 2, as the level of contamination increases, the performance gap between cellGMM and its competitors becomes evident. Indeed, with 10% of contamination, cellGMM maintains good classification results, while the performance of the competitors deteriorates. Additional results can be found in Section 3.1 of the Supplementary Material.

4.2 Carina Nebula Data Set

The proposed methodology is also suitable for image reconstruction. In this framework, we evaluate the detection and “correction” of contaminated cells through their imputation. Specifically, we analyze an image captured by the James Webb Space Telescope, which depicts the edge of NGC 3324 located in the northwest corner of the Carina Nebula. The image of the stars’ birth is available at <https://science.nasa.gov/universe/stars/>. The original picture has 1600×927 pixels (Figure 4a), corresponding to more than one million units

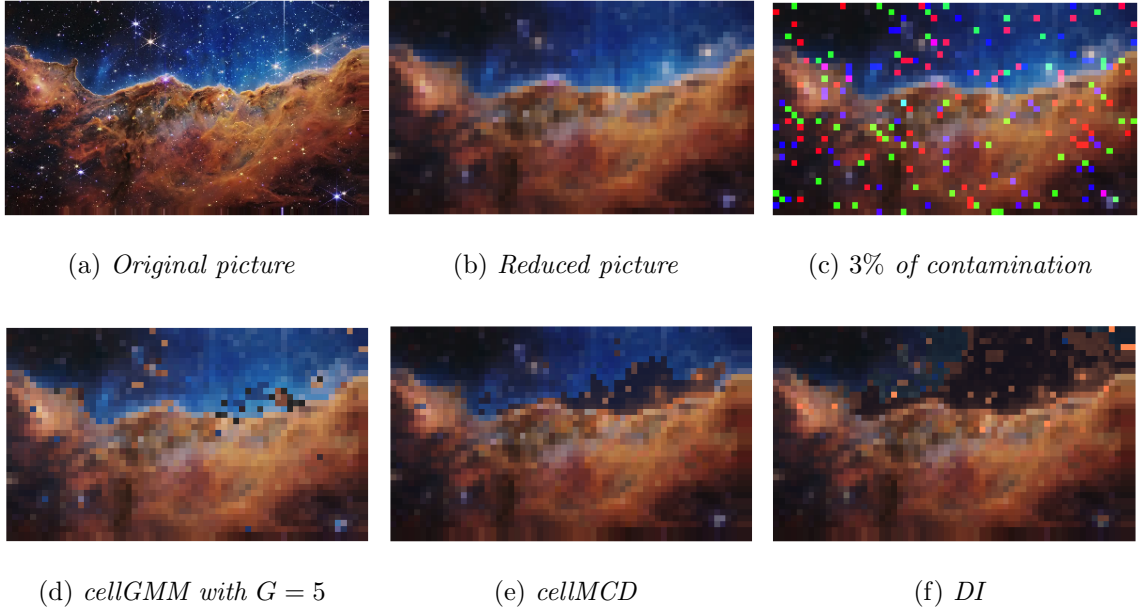


Figure 4: Carina Nebula birth. The methods' imputation are shown in (d)-(f).

measured in three variables (RGB). Due to its high size, we reduce it into 60×35 pixels (Figure 4b), which we then corrupt with 3% of contamination, as depicted in Figures 4c and 5a.

Given our goal, the most appropriate methods to compare to cellGMM are cellMCD and DI, as they provide imputation for contaminated cells. As shown in Figures 4d-4f and 5b-5d, cellGMM demonstrates better potential in image reconstruction than the single-population methods. Moreover, as expected, the higher the number of components, the better the classification performance of cellGMM. This is evident by considering the RMSE between the imputed and the original data sets, which is 0.073 for cellGMM with $G = 2$ and 0.059 for cellGMM with $G = 5$, both lower than 0.079 for cellMCD and 0.127 for DI.

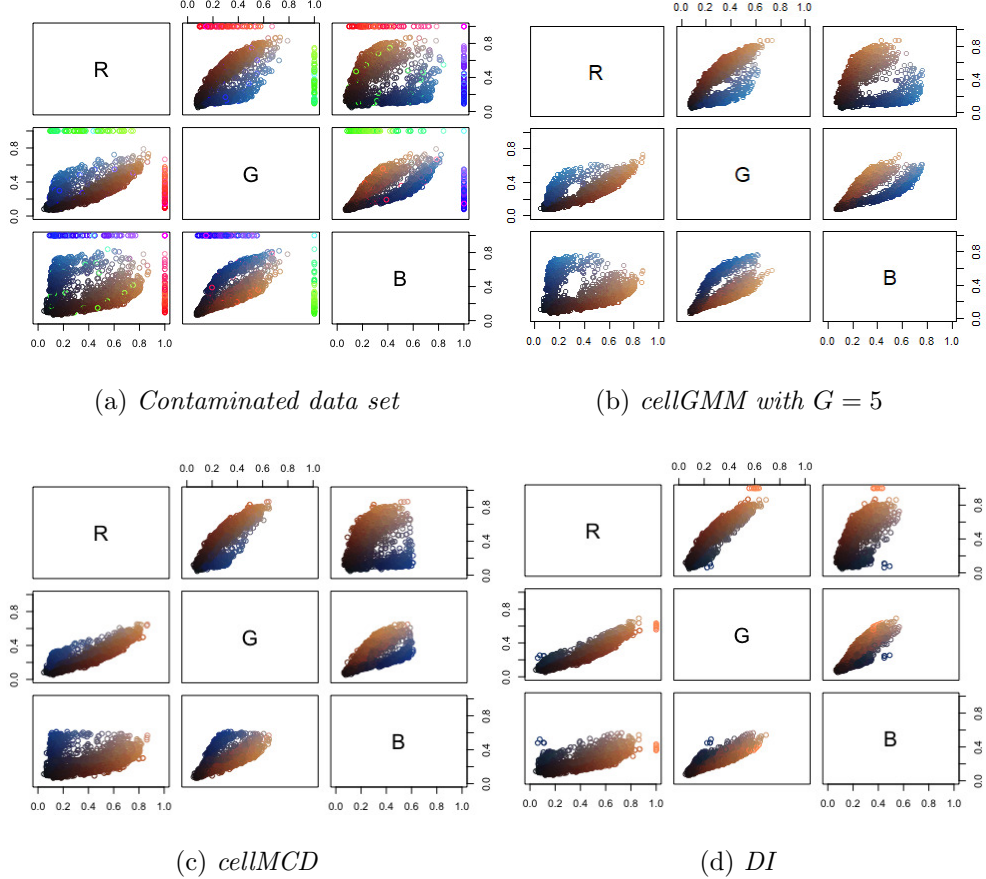


Figure 5: Pair plots of the Carina Nebula data set. The methods' imputation are shown in (b)-(d).

4.3 Top Gear Data Set

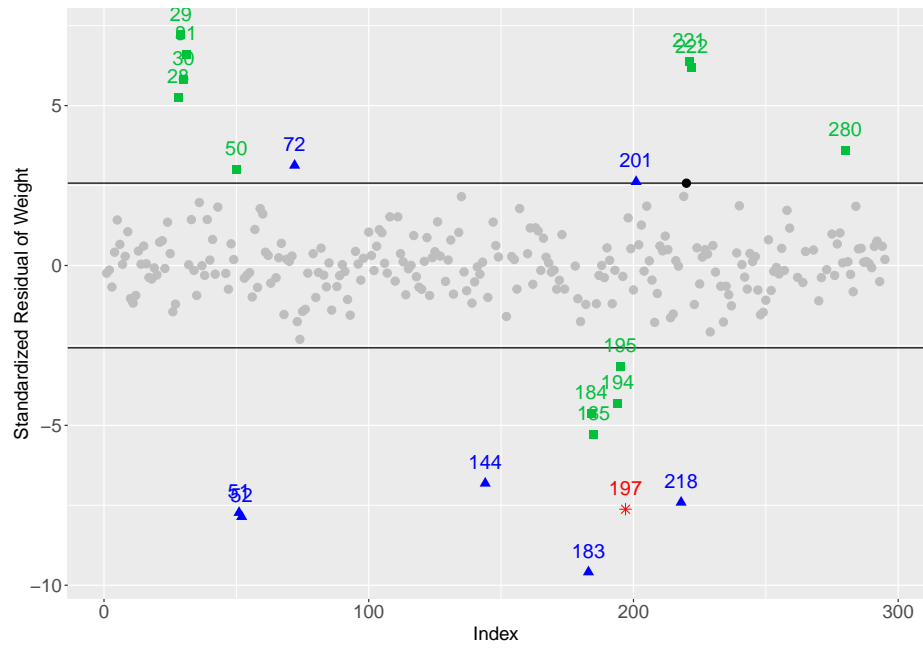
In this section, we analyze the car data set available in the R package `robustHD` (Alfons, 2021), called *TopGear*, which contains authentic missing values (2.74% of the cells) and potential outliers. We focus on the eleven numerical variables by removing the two cars with more missing than observed values, resulting in a final sample size of $n = 295$, and transforming the highly skewed variables using their logarithms, as reported in Raymaekers and Rousseeuw (2023). Unlike these authors, we provide a cluster-oriented approach to this

Table 3: Ten representative cars per cluster

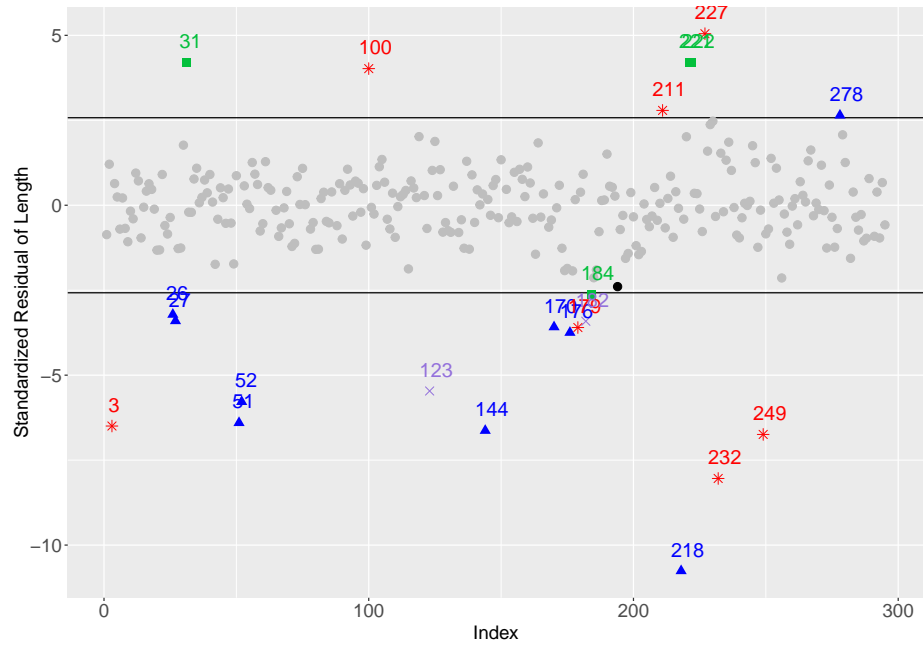
Cluster 1	Cluster 2	Cluster 3	Cluster 4
Audi A4	Chevrolet Spark	Aston Martin DB9	BMW X5
Jaguar XF Sportbrake	Hyundai i10	Aston Martin DB9 Volante	BMW X6
Kia Optima	Kia Picanto	Aston Martin V12 Zagato	Hyundai i800
Lexus GS	Peugeot 107	Aston Martin Vanquish	Jeep Grand Cherokee
Mercedes-Benz E-Class Coupé	Proton Savvy	Aston Martin Vantage	Land Rover Discovery 4
Skoda Octavia	SEAT Mii	Aston Martin Vantage Roadster	Land Rover Range Rover
Vauxhall Cascada	Suzuki Alto	Audi R8	Mercedes-Benz G-Class
Vauxhall Insignia Sports Tourer	Toyota AYGO	Audi R8 V10	Mercedes-Benz GL-Class
Volkswagen CC	Toyota iQ	Bentley Continental	Porsche Cayenne
Volkswagen Passat	Volkswagen Up	Bentley Continental GTC	Toyota Land Cruiser V8

data set by setting $G = 4$, which identifies meaningful groups with distinct features. The cars are divided into “compact and mid-size sedans and crossovers” (Cluster 1); “economy and city cars” (Cluster 2); “luxury and high-performance cars” (Cluster 3); “large SUVs and off-roaders” (Cluster 4). A list of ten representative cars per cluster, selected as those with the highest posterior probabilities, is provided in Table 3, while a comprehensive overview of the clusters is reported in Section 3.2 of the Supplementary Material.

All the variables are affected by unreliable cells, particularly *Weight* (17.63%), *Width* (11.86%), *Length* (11.19%), *Height* (11.19%), *MPG* (8.47%), and *ln(Price)* (8.14%). For the other five variables, i.e., *ln(Displacement)*, *ln(BHP)*, *ln(Torque)*, *Acceleration* and *ln(TopSpeed)*, the percentage of reliable cells ranges from 94% to 99% and refers to both contaminated and missing values, except for *ln(Price)* and *Acceleration*, which are fully observed. Considering separately the four variables mostly affected by unreliable cells, Figure 6 shows the standardized cellwise residuals, calculated as $(x_{ij} - \hat{x}_{ij(g)})/\sqrt{\hat{C}_{ij(g)}}$, where

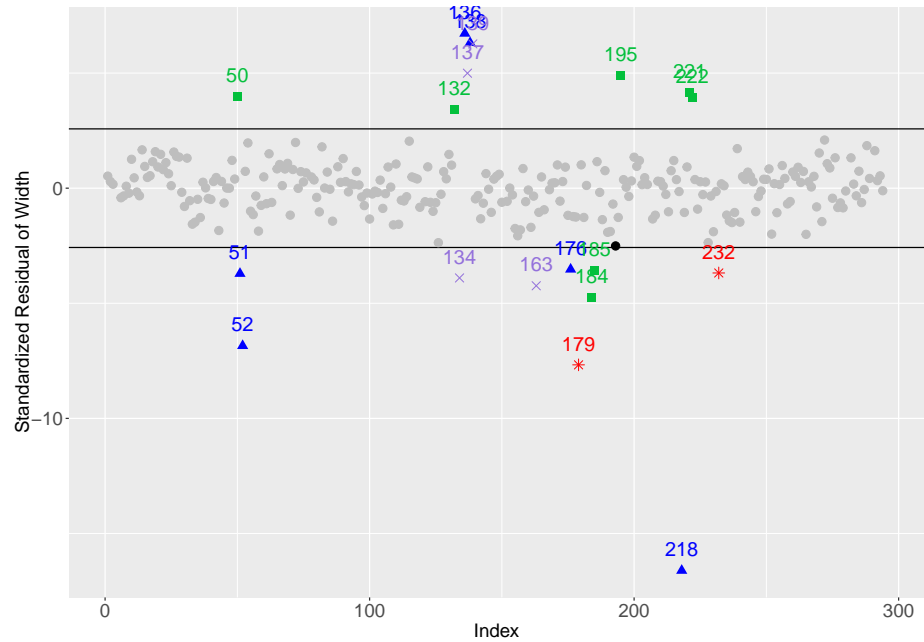


(a) *Weight*

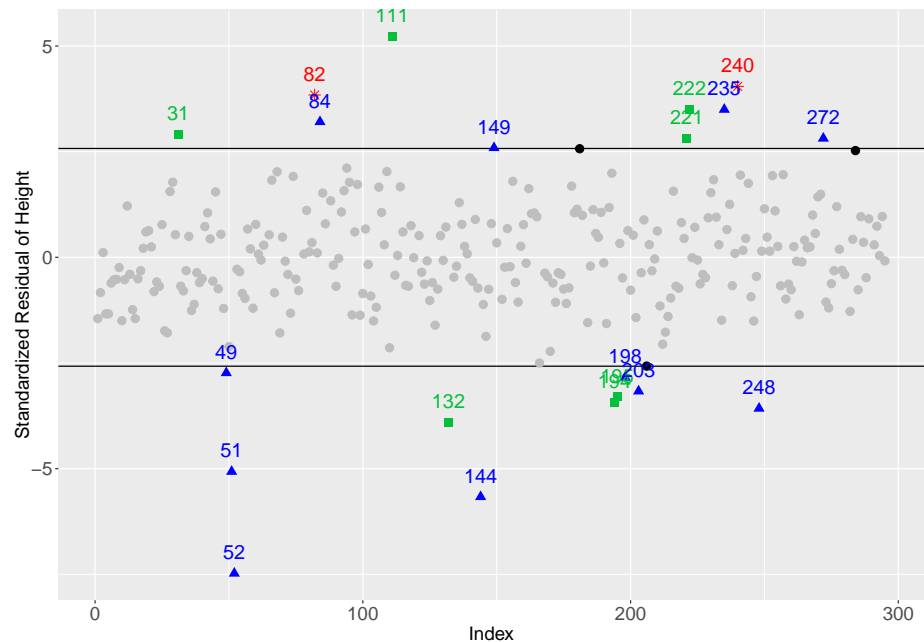


(b) *Length*

Figure 6: Top Gear data set: index plot of the standardized residuals per variable (Cluster 1: blue - triangle; Cluster 2: red - asterisk; Cluster 3: green - square; Cluster 4: purple - cross)



(c) *Width*



(d) *Height*

Figure 6: Top Gear data set: index plot of the standardized residuals per variable (Cluster 1: blue - triangle; Cluster 2: red - asterisk; Cluster 3: green - square; Cluster 4: purple - cross)

Table 4: Top Gear data set: ID and name of the cars resulting with high standardized residuals in absolute terms

ID	Car name	ID	Car name	ID	Car name	ID	Car name
3	Aston Martin Cygnet	84	Fiat Doblo	170	Mercedes-Benz SLK	211	Proton GEN-2
26	Audi TT Coupe	100	Honda Insight	176	Mini John Cooper Works	218	Renault Twizy
27	Audi TT Roadster	111	Infiniti EX	179	Mitsubishi i-MiEV	221	Rolls-Royce Phantom
28	Bentley Continental	123	Jeep Wrangler	182	Mitsubishi Shogun	222	Rolls-Royce Phantom Coupe
29	Bentley Continental GTC	132	Lamborghini Aventador	183	Morgan 3 Wheeler	227	SEAT Toledo
30	Bentley Flying Spur	134	Land Rover Defender	184	Morgan Aero	232	Smart fortwo
31	Bentley Mulsanne	136	Land Rover Freelander 2	185	Morgan Roadster	235	Subaru Forester
49	BMW Z4	137	Land Rover Range Rover	194	Noble M600	240	Suzuki Jimny
50	Bugatti Veyron	138	Land Rover Range Rover Evoque	195	Pagani Huayra	248	Toyota GT 86
51	Caterham CSR	139	Land Rover Range Rover Sport	197	Peugeot 107	249	Toyota iQ
52	Caterham Super 7	144	Lotus Elise	198	Peugeot 207 CC	272	Vauxhall Zafira Tourer
72	Citroen DS5	149	Mazda CX-5	201	Peugeot 3008	278	Volkswagen Jetta
82	Fiat 500L	163	Mercedes-Benz G-Class	203	Peugeot 308 CC	280	Volkswagen Phaeton

$g = \arg \max_{g'=1, \dots, G} \hat{z}_{ig'}$. Missing data are not displayed in the plots, and the horizontal lines represent $\pm \sqrt{\chi^2_{1,0.99}}$. For instance, the Bentley Continental, Bentley Continental GCT, Bentley Mulsanne, Flying Spur, Rolls-Royce Phantom, Rolls-Royce Phantom Coupé, and Volkswagen Phaeton feature soundproofing materials and structural reinforcements that increase their weight, among other features (Figure 6a); the Aston Martin Cygnet, Smart fortwo, and Toyota iQ are shorter than typical city cars, whereas the SEAT Toledo, Honda Insight, and Proton GEN-2 are longer (Figure 6b). Other examples are the Land Rover Range Rover and Land Rover Range Rover Sport for Cluster 4, which have a width greater than expected for large SUVs or off-roaders (Figure 6c), while the Fiat Doblo and Subaru Forester have a height higher than that of crossovers (Figure 6d). It should be noted that for each variable, some cars may not be marginal outliers but could still be flagged as

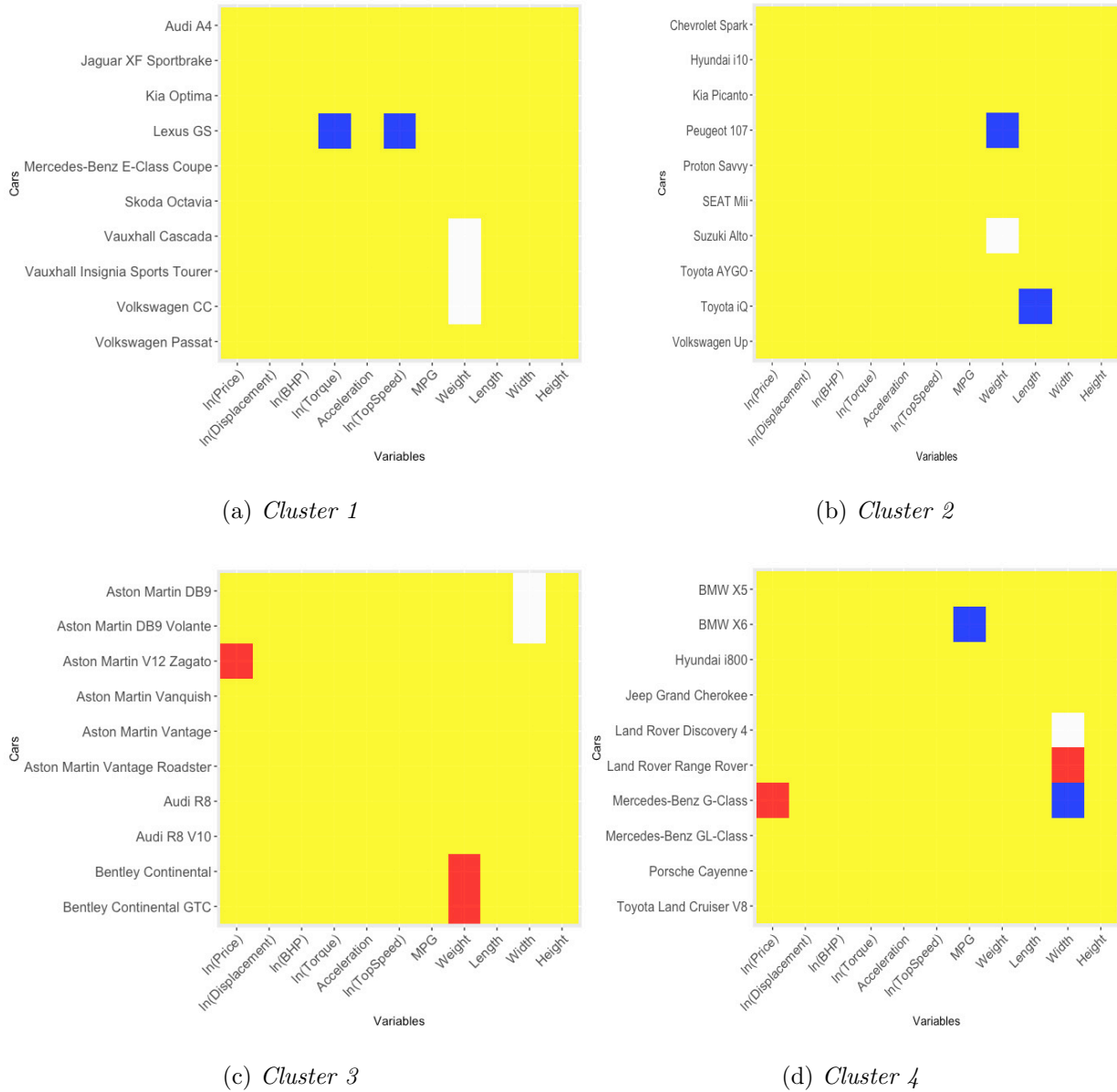


Figure 7: Top Gear data set: representation of cellwise outliers and their imputation for the ten representative cars per cluster. Yellow: reliable cells; blue: contaminated cells imputed with a higher value than the original one; red: contaminated cells imputed with a lower value than the original one; white: missing values

contaminated by cellGMM (black points in Figure 6) based on the cluster configuration, meaning they might actually be points lying between clusters. Finally, an illustration of the unreliable cells for the most representative cars per cluster, as listed in Table 3, is shown in Figure 7. Here, it is notable that some cars, such as the Peugeot 107 in Cluster 2, display only one contaminated cell, whereas others have multiple. For instance, conditional on their other 9 variables, the Lexus GS in Cluster 1 has $\ln(\text{Torque})$ and $\ln(\text{Top Speed})$ significantly lower than expected in the cluster including mostly mid-side sedans (Figure 7a), and the Mercedes-Benz G-Class, although more expensive than expected for off-roaders, has a lower width (Figure 7d).

5 Discussion

The cellGMM methodology introduced in this paper is designed to detect and handle contaminated cells in heterogeneous populations, as well as manage missing values. Following the new paradigm of cellwise contamination and the rationale of the EM, we have proposed an algorithm that includes a concentration step to identify unreliable cells before the E- and M-steps, where the corresponding values are imputed and the Gaussian mixture model parameters are estimated, respectively. The estimation is constrained to ensure robustness and avoid degeneracies and spurious solutions. Compared to the existing methodology for model-based clustering in the presence of cellwise adulteration, cellGMM leverages the relationships among variables – especially when they are strong – by imputing the unreliable cells. In contrast, sclust sets these cells to NA in the parameter estimation.

While the proposal was initially illustrated by constraining the same proportion of con-

taminated cells per variable, a penalized version of cellGMM allows for automatic adjustments to avoid discarding valuable information and improve efficiency. The performance of these two approaches, in terms of clustering, parameter recovery, and data imputation, has been tested in a simulation study where cellGMM was compared to other robust and non-robust methodologies across both single and heterogeneous population frameworks. The examined scenarios cover simple and complex situations, considering different cluster configurations (well-separated and close components), data dimensionality (smaller and higher), outlier generation and magnitude (less and more extreme), and information removal (missing data). Additionally, three real data applications illustrate the results of cellGMM in different fields and for various purposes, such as the classification of spectral data, image reconstruction, and outlier detection in a data set where contaminated and missing values are not artificially generated. These are a few examples of possible applications of cellGMM, which can be implemented in any domain where the goal is to cluster data affected by missing information and potential outlying values within the variables.

Notwithstanding the results shown throughout the paper, several issues remain open for future research as the proposal is one of the first attempts to handle cellwise outlier detection in mixture models. First and foremost, we will delve into a criterion for selecting the number of components, which is rather fixed in our experiments. This criterion should account for the number of cells detected as contaminated, which can vary in the penalized approach. It is worth noting that cellGMM was developed under a frequentist framework, but it could potentially be developed within a Bayesian framework, where the number of mixture components might be estimated directly within the model, as in an infinite

Gaussian mixture model (Ferguson, 1973). Moreover, although the proposal can sometimes handle heavy tails through the cellwise approach, it is not explicitly designed to address skewed and/or multi-modal cluster distributions. This limitation could be addressed by extending the model to assume a t distribution for each mixture component in a frequentist approach, or by considering infinite mixture of infinite Gaussian mixtures, as proposed by Yerebakan et al. (2014) in a Bayesian context. Additionally, the procedure for the initialization of the cellGMM algorithm may be improved by performing a detailed study on the tuning parameter settings to balance performance and avoid trapping initial solutions in specific regions of the parameter space. Finally, the cellwise properties of the parameter estimators will be theoretically inspected.

Supplementary Materials

Supplementary Material: This .pdf file contains insights into the cellGMM algorithm, including computations for the E- and M-step, initialization, and monotonicity (Section 1); additional results from the simulation study, along with computational time and complexity (Section 2); and from real data applications (Section 3).

Code: R code for the implementation of cellGMM and replication of the analyses in Section 3 (Figures 1-2 and Table 1) and the results in Section 4.2 (Figure 5) is available in the .zip file and at <https://github.com/giorgiazaccaria/cellGMM>.

Data: The sources for the Carina Nebula and Top Gear data sets are reported in Sections 4.2 and 4.3, respectively, while the Homogenized Meat data set is available in the Supplemental Content of Murphy et al. (2010).

Acknowledgments

The Authors sincerely thank the Editor, Associate Editor and two anonymous Reviewers for their constructive comments and suggestions.

Disclosure Statement

The authors report there are no competing interests to declare.

Funding

The research of Giorgia Zaccaria and Francesca Greselin was supported by Milano-Bicocca University Fund for Scientific Research, 2023-ATE-0448. Francesca Greselin's research was also supported by PRIN2022 - 2022LANNKC. The research of Luis A. García-Escudero and Agustín Mayo-Íscar was partially supported by grant PID2021-128314NB-I00 funded by MCIN/AEI/10.13039/501100011033/FEDER, UE and Junta Castilla y León grant VA064G24.

References

Alfons, A. (2021), “robustHD: An R package for robust regression with high-dimensional data,” *Journal of Open Source Software*, 6, 3786.

Alqallaf, F., Van Aelst, S., Yohai, V. J., and Zamar, R. H. (2009), “Propagation of outliers in multivariate data,” *The Annals of Statistics*, 37, 311–331.

Böhning, D., Dietz, E., Schaub, R., Schlattmann, P., and Lindsay, B. (1994), “The distribu-

tion of the likelihood ratio for mixtures of densities from the one-parameter exponential family,” *Annals of the Institute of Statistical Mathematics*, 46, 373–388.

Cappozzo, A., Greselin, F., and Murphy, T. B. (2021), “Robust variable selection for model-based learning in presence of adulteration,” *Computational Statistics & Data Analysis*, 158, 107186.

Cuesta-Albertos, J. A., Gordaliza, A., and Matran, C. (1997), “Trimmed k -means: An attempt to robustify quantizers,” *The Annals of Statistics*, 25, 553–576.

Dempster, A. P., Laird, N. M., and Rubin, D. B. (1977), “Maximum likelihood from incomplete data via the EM algorithm,” *Journal of the Royal Statistical Society, Series B (Statistical Methodology)*, 39, 1–38.

Farcomeni, A. (2013), “Snipping for robust k -means clustering under component-wise contamination,” *Statistics and Computing*, 24, 907–919.

— (2014), “Robust constrained clustering in presence of entry-wise outliers,” *Technometrics*, 56, 102–111.

Ferguson, T. S. (1973), “A bayesian analysis of some nonparametric problems,” *The Annals of Statistics*, 1, 209–230.

García-Escudero, L. A., Gordaliza, A., Matrán, C., and Mayo-Iscar, A. (2008), “A general trimming approach to robust cluster analysis,” *The Annals of Statistics*, 36, 1324–1345.

García-Escudero, L. A., Gordaliza, A., and Mayo-Iscar, A. (2014), “A constrained robust

proposal for mixture modeling avoiding spurious solutions,” *Advances in Data Analysis and Classification*, 8, 27–43.

García-Escudero, L. A., Rivera-García, D., Mayo-Iscar, A., and Ortega, J. (2021), “Cluster analysis with cellwise trimming and applications for the robust clustering of curves,” *Information Sciences*, 573, 100–124.

Ghahramani, Z. and Jordan, M. (1995), “Learning from incomplete data,” Technical Report AI Lab Memo No. 1509, CBCL Paper No. 108, MIT AI Lab.

Huber, P. J. (1964), “Robust estimation of a location parameter,” *The Annals of Mathematical Statistics*, 35, 73–101.

Hubert, M., Rousseeuw, P. J., and den Bossche, W. V. (2019), “MacroPCA: An all-in-one PCA method allowing for missing values as well as cellwise and rowwise outliers,” *Technometrics*, 61, 459–473.

Little, R. J. A. and Rubin, D. B. (2019), *Statistical Analysis with Missing Data*, 3rd ed., John Wiley & Sons, Hoboken.

Maitra, R. and Melnykov, V. (2010), “Simulating data to study performance of finite mixture modeling and clustering algorithms,” *Journal of Computational and Graphical Statistics*, 19, 354–376.

McElhinney, J., Downey, G., and Fearn, T. (1999), “Chemometric processing of visible and near infrared reflectance spectra for species identification in selected raw homogenised meats,” *Journal of Near Infrared Spectroscopy*, 7, 145–154.

McLachlan, G. J. and Krishnan, T. (2008), *The EM algorithm and extensions*, 2nd ed., Wiley, Hoboken.

McLachlan, G. J. and Peel, D. (2000), *Finite mixture models*, Wiley, New York.

Murphy, T. B., Dean, N., and Raftery, A. E. (2010), “Variable selection and updating in model-based discriminant analysis for high dimensional data with food authenticity applications,” *The Annals of Applied Statistics*, 4, 396–421.

Neykov, N. M., Filzmoser, P., Dimova, R., and Neytchev, P. N. (2007), “Robust fitting of mixtures using the trimmed likelihood estimator,” *Computational Statistics & Data Analysis*, 52, 299–308.

Peel, D. and McLachlan, G. J. (2000), “Robust mixture modelling using the t distribution,” *Statistics and Computing*, 10, 339–348.

Punzo, A. and McNicholas, P. D. (2016), “Parsimonious mixtures of multivariate contaminated normal distributions,” *Biometrical Journal*, 58, 1506–1537.

Raymaekers, J. and Rousseeuw, P. J. (2021), “Handling cellwise outliers by sparse regression and robust covariance,” *Journal of Data Science, Statistics, and Visualisation*, 1, <https://doi.org/10.52933/jdssv.v1i3.18>.

— (2023), “The cellwise minimum covariance determinant estimator,” *Journal of the American Statistical Association*, 119, 2610–2621.

— (2024), “Challenges of cellwise outliers,” *Econometrics and Statistics*, <https://doi.org/10.1016/j.ecosta.2024.02.002>.

Rousseeuw, P. J. (1984), “Least median of squares regression,” *Journal of the American Statistical Association*, 79, 871–880.

— (1985), “Multivariate estimation with high breakdown point,” in *Mathematical Statistics and Applications*, eds. W. Grossmann, G. Pflug, I. Vincze, and W. Wertz, pp. 283–297.

Rousseeuw, P. J. and van Driessen, K. (1999), “A fast algorithm for the minimum covariance determinant estimator,” *Technometrics*, 41, 212–223.

Rubin, D. B. (1976), “Inference and missing data,” *Biometrika*, 63, 581–592.

Tong, H. and Tortora, C. (2022), “Model-based clustering and outlier detection with missing data,” *Advances in Data Analysis and Classification*, 16, 5–30.

Wang, H., Zhang, Q., Luo, B., and Wei, S. (2004), “Robust mixture modelling using multivariate t-distribution with missing information,” *Pattern Recognition Letters*, 25, 701–710.

Yao, W. (2015), “Label switching and its solutions for frequentist mixture models,” *Journal of Statistical Computation and Simulation*, 85, 1000–1012.

Yerebakan, H. Z., Rajwa, B., and MuratDundar (2014), “The infinite mixture of infinite gaussian mixtures,” in *Advances in Neural Information Processing Systems*, eds. Z. Ghahramani, M. Welling, C. Cortes, N. Lawrence, and K. Weinberger, vol. 27, Curran Associates, Inc.

Supplementary Material to “Cellwise outlier detection in heterogeneous populations”

Giorgia Zaccaria¹, Luis A. García-Escudero², Francesca Greselin¹,
and Agustín Mayo-Íscar²

¹Department of Statistics and Quantitative Methods
University of Milano-Bicocca

²Department of Statistics and Operational Research
University of Valladolid

This document includes the supplementary material to the main article “Cellwise outlier detection in heterogeneous populations”. Specifically, Section 1 provides details on the cellGMM algorithm. Additional scenarios for the simulation study are presented in Section 2, along with the computational time and complexity of the proposed methodology. Finally, Section 3 contains an in-depth analysis of the Homogenized Meat data set and the Top Gear data set examined in the main article.

1 Details on the cellGMM algorithm

1.1 Computations for the E- and M-step

In this section, we illustrate the computations required in the E- and M-step of the cell-GMM algorithm. In the E-step, we compute the expected values $\mathbb{E}[Z_{ig}|\mathbf{x}_{i[\mathbf{w}_i^{(t+1)}]}; \widehat{\boldsymbol{\Psi}}^{(t)}]$, $\mathbb{E}[\mathbf{X}_{i[\mathbf{w}_i^{(t+1)c}]}|\mathbf{x}_{i[\mathbf{w}_i^{(t+1)}]}, z_{ig} = 1; \widehat{\boldsymbol{\Psi}}^{(t)}]$ and $\mathbb{E}[(\mathbf{X}_{i[\mathbf{w}_i^{(t+1)c}]} - \boldsymbol{\mu}_{g[\mathbf{w}_i^{(t+1)c}]}) (\mathbf{X}_{i[\mathbf{w}_i^{(t+1)c}]} - \boldsymbol{\mu}_{g[\mathbf{w}_i^{(t+1)c}]})']$

$|\mathbf{x}_{i[\mathbf{w}_i^{(t+1)}]}, z_{ig} = 1; \widehat{\boldsymbol{\Psi}}^{(t)}]$, which can be easily derived following Ghahramani and Jordan (1995):

$$\mathbb{E}[Z_{ig}|\mathbf{x}_{i[\mathbf{w}_i^{(t+1)}]}; \widehat{\boldsymbol{\Psi}}^{(t)}] = \frac{\widehat{\pi}_g^{(t)} \phi_{p[\mathbf{w}_i^{(t+1)}]}(\mathbf{x}_{i[\mathbf{w}_i^{(t+1)}]}; \widehat{\boldsymbol{\mu}}_{g[\mathbf{w}_i^{(t+1)}]}^{(t)}, \widehat{\boldsymbol{\Sigma}}_{g[\mathbf{w}_i^{(t+1)}, \mathbf{w}_i^{(t+1)}]}^{(t)})}{\sum_{h=1}^G \widehat{\pi}_h^{(t)} \phi_{p[\mathbf{w}_i^{(t+1)}]}(\mathbf{x}_{i[\mathbf{w}_i^{(t+1)}]}; \widehat{\boldsymbol{\mu}}_{h[\mathbf{w}_i^{(t+1)}]}^{(t)}, \widehat{\boldsymbol{\Sigma}}_{h[\mathbf{w}_i^{(t+1)}, \mathbf{w}_i^{(t+1)}]}^{(t)})} := z_{ig}^{(t+1)} \quad (1)$$

$$\begin{aligned} \mathbb{E}[\mathbf{X}_{i[\mathbf{w}_i^{(t+1)c}]}|\mathbf{x}_{i[\mathbf{w}_i^{(t+1)}]}, z_{ig} = 1; \widehat{\boldsymbol{\Psi}}^{(t)}] &= \widehat{\boldsymbol{\mu}}_{g[\mathbf{w}_i^{(t+1)c}]}^{(t)} + \widehat{\boldsymbol{\Sigma}}_{g[\mathbf{w}_i^{(t+1)c}, \mathbf{w}_i^{(t+1)}]}^{(t)} (\widehat{\boldsymbol{\Sigma}}_{g[\mathbf{w}_i^{(t+1)}, \mathbf{w}_i^{(t+1)}]}^{(t)})^{-1} \\ &(\mathbf{x}_{i[\mathbf{w}_i^{(t+1)}]} - \widehat{\boldsymbol{\mu}}_{g[\mathbf{w}_i^{(t+1)}]}^{(t)}) := \widehat{\mathbf{x}}_{i[\mathbf{w}_i^{(t+1)c}](g)}^{(t+1)} \end{aligned} \quad (2)$$

$$\begin{aligned} \mathbb{E}[(\mathbf{X}_{i[\mathbf{w}_i^{(t+1)c}]} - \boldsymbol{\mu}_{g[\mathbf{w}_i^{(t+1)c}]})(\mathbf{X}_{i[\mathbf{w}_i^{(t+1)c}]} - \boldsymbol{\mu}_{g[\mathbf{w}_i^{(t+1)c}]}')'|\mathbf{x}_{i[\mathbf{w}_i^{(t+1)}]}, z_{ig} = 1; \widehat{\boldsymbol{\Psi}}^{(t)}] &= \widetilde{\mathbf{C}}_{i(g)}^{(t+1)} + \widetilde{\mathbf{C}}_{i(g)}^{\approx} \end{aligned} \quad (3)$$

where $\widetilde{\mathbf{C}}_{i(g)}^{(t+1)} := \widehat{\boldsymbol{\Sigma}}_{g[\mathbf{w}_i^{(t+1)c}, \mathbf{w}_i^{(t+1)c}]}^{(t)} - \widehat{\boldsymbol{\Sigma}}_{g[\mathbf{w}_i^{(t+1)c}, \mathbf{w}_i^{(t+1)}]}^{(t)} (\widehat{\boldsymbol{\Sigma}}_{g[\mathbf{w}_i^{(t+1)}, \mathbf{w}_i^{(t+1)}]}^{(t)})^{-1} \widehat{\boldsymbol{\Sigma}}_{g[\mathbf{w}_i^{(t+1)}, \mathbf{w}_i^{(t+1)c}]}^{(t)}$ and $\widetilde{\mathbf{C}}_{i(g)}^{\approx} \approx \left(\widehat{\mathbf{x}}_{i[\mathbf{w}_i^{(t+1)c}](g)}^{(t+1)} - \widehat{\boldsymbol{\mu}}_{g[\mathbf{w}_i^{(t+1)c}]}^{(t)} \right) \left(\widehat{\mathbf{x}}_{i[\mathbf{w}_i^{(t+1)c}](g)}^{(t+1)} - \widehat{\boldsymbol{\mu}}_{g[\mathbf{w}_i^{(t+1)c}]}^{(t)} \right)'$.

The M-step provides the parameter estimates by considering the *completed* data $\left\{ \left\{ \tilde{\mathbf{x}}_{i(g)}^{(t+1)} = (\mathbf{x}_{i[\mathbf{w}_i^{(t+1)}]}, \widehat{\mathbf{x}}_{i[\mathbf{w}_i^{(t+1)c}](g)}^{(t+1)})' \right\}_{g=1}^G \right\}_{i=1}^n$.

Update of $\boldsymbol{\pi}$. The weights $\boldsymbol{\pi} = \{\pi_g\}_{g=1}^G$ are updated as

$$\widehat{\pi}_g^{(t+1)} = \frac{\sum_{i=1}^n z_{ig}^{(t+1)}}{n}. \quad (4)$$

Update of $\boldsymbol{\theta}$. The component mean vectors and covariance matrices in $\boldsymbol{\theta} = \{\boldsymbol{\mu}_g, \boldsymbol{\Sigma}_g\}_{g=1}^G$

are updated as

$$\widehat{\boldsymbol{\mu}}_g^{(t+1)} = \frac{\sum_{i=1}^n z_{ig}^{(t+1)} \tilde{\mathbf{x}}_{i(g)}^{(t+1)}}{\sum_{i=1}^n z_{ig}^{(t+1)}}, \quad (5)$$

$$\widehat{\boldsymbol{\Sigma}}_g^{(t+1)} = \frac{\sum_{i=1}^n z_{ig}^{(t+1)} \left[(\tilde{\mathbf{x}}_{i(g)}^{(t+1)} - \widehat{\boldsymbol{\mu}}_g^{(t+1)}) (\tilde{\mathbf{x}}_{i(g)}^{(t+1)} - \widehat{\boldsymbol{\mu}}_g^{(t+1)})' + \widetilde{\mathbf{C}}_{i(g)}^{(t+1)} \right]}{\sum_{i=1}^n z_{ig}^{(t+1)}}. \quad (6)$$

If the eigenvalue-ratio constraint is not satisfied, truncated eigenvalues that comply with the constraint are obtained using the efficient procedure proposed by Fritz et al. (2013). The corresponding component covariance matrices are then computed by substituting the truncated eigenvalues into their singular value decomposition.

1.2 Initialization

The procedure proposed for the initialization of the cellGMM algorithm is detailed below. This is heavily based on several applications of the TCLUST method, which is implemented via the R package `tclust` (Fritz et al., 2012).

Step 1 **Initialization of \mathbf{W} :** the initial solution for \mathbf{W} is obtained by applying TCLUST individually to each variable and to pairs of variables with a fixed α_{tclust} trimming level. The estimated parameters per component from these TCLUST applications are used to compute the Mahalanobis distances. Roughly speaking, the smallest Mahalanobis distance across components for each unit is considered in both univariate and bivariate TCLUST applications. Proportions α_1 and α_2 of cells per variable are flagged as outliers based on the distribution of the Mahalanobis distances computed via univariate and bivariate TCLUST, respectively. Unreliable cells per variable previously identified through univariate TCLUST are excluded from the bivariate TCLUST outlier detection. A more detailed pseudo-code description of this procedure is provided in Algorithm 1. Notice that in the pseudo-code we refer to the Mahalanobis distances as MD.

Step 2 Initialization of Ψ :

2.1 n_{rep} subsets of q out of p variables are randomly selected. For each reduced set of q variables, TCLUST is implemented with a fixed trimming level α_{A_1} on the resulting completely reliable observations to obtain G component mean vectors and covariance matrices. It is worth noting that reducing the set of variables considered increases the number of completely reliable observations as input for TCLUST, where the reliability of an observation is based upon the initial configuration of \mathbf{W} (see Step 1). The two sets composed of n_{rep} parameters each resulting from TCLUST are stored into \mathbf{tclust}_μ (n_{rep} location vectors) and \mathbf{tclust}_Σ (n_{rep} scatter matrices), respectively.

2.2 In this part, a version of trimmed k -means (Cuesta-Albertos et al., 1997) accommodated for the presence of missing values is implemented to obtain a partition of the n_{rep} elements in \mathbf{tclust}_μ into G groups. The corresponding “centers of centers” are then used to initialize $\{\boldsymbol{\mu}_g\}_{g=1}^G$. Specifically, according to a multi-start procedure, a matrix \mathbf{N} representing G centers of center groups is initialized by one of the n_{rep} elements in \mathbf{tclust}_μ . Then, \mathbf{N} is iteratively updated across n_{iter} iterations by assigning the n_{rep} elements in \mathbf{tclust}_μ to the nearest center of centers in \mathbf{N} and recomputing \mathbf{N} accordingly. The latter is obtained as the mean of centers in \mathbf{tclust}_μ per group, after having discarded a proportion α_{A2} of them according to their squared Euclidean distances. Among several random starts (n_{start}), the selected solution for $\{\boldsymbol{\mu}_g\}_{g=1}^G$ is \mathbf{N} that minimizes the total squared Euclidean distances between the centers in \mathbf{tclust}_μ and the centers of

center groups in \mathbf{N} . The resulting partition in groups is also used for computing the G component covariance matrices $\{\Sigma_g\}_{g=1}^G$ as the means of the elements in tclust_Σ per group. It is worth noting that this procedure does not necessarily guarantee the positive definiteness of Σ_g , as the mean of covariance matrices in tclust_Σ refers to different subsets of variables. Therefore, we impose on $\{\Sigma_g\}_{g=1}^G$ the eigenvalue-ratio constraint reported in (4) of the main article, which entails obtaining positive definite matrices. This constraint is implemented throughout the cellGMM algorithm via the efficient procedure reported in Fritz et al. (2013). The weights $\boldsymbol{\pi} = \{\pi_g\}_{g=1}^G$ are figured up after assigning each observation to a component by considering the minimum squared Euclidean distance from $\{\boldsymbol{\mu}_g\}_{g=1}^G$. A more detailed pseudo-code description of the procedure proposed in this Step 2.2 is illustrated in Algorithm 2.

The initialization described herein depends on several tuning parameters. In our experiments, we set those regarding the trimming levels according to the true level of contamination, denoted as α_{true} . Specifically, we set $\alpha_{\text{tclust}} = 2 \cdot \alpha_{\text{true}}$, $\alpha_1 = \alpha_2 = \alpha_{\text{true}}$, $\alpha_{A1} = \alpha_{\text{true}}$ and $\alpha_{A2} = 2 \cdot \alpha_{\text{true}}$. If α_{true} is unknown, as it is usually the case in real-world applications, we suggest considering a conservative level of contamination as the true value, e.g., 0.03 or 0.05 (i.e., assuming 3% or 5% of contamination). The tuning parameter q , which controls the number of variables selected in the first step of the initialization of $\boldsymbol{\Psi}$, is fixed to $\lfloor \frac{p}{2} \rfloor + 1$. This choice guarantees that the subsets of sampled variables overlap for at least one variable. The remaining parameters for the initialization of $\boldsymbol{\Psi}$ are set as follows: $n_{\text{rep}} = 40$, $n_{\text{start}} = 10$ and $n_{\text{iter}} = 10$. This configuration of the tuning parameters proves to

be effective in our experiments. However, their setting could be improved by performing a specific simulation study on the initialization, which is out of the scope of this paper primarily focused on the main part of the cellGMM algorithm.

1.3 Algorithm monotonicity

In the following theorem, we state the monotonicity of the cellGMM algorithm.

Theorem 1. *The cellGMM objective function, subject to the constraint on the number of reliable cells per variable and the eigenvalue-ratio constraint, is non-decreasing at each iteration of the EM-type algorithm.*

Proof. We first show the monotonicity of the log-likelihood, i.e., $\ell(\widehat{\Psi}^{(t+1)}, \mathbf{W}^{(t+1)}; \mathbf{X}) \geq \ell(\widehat{\Psi}^{(t)}, \mathbf{W}^{(t)}; \mathbf{X}), \forall t = 0, 1, 2, \dots$. To establish this, we need to verify that the log-likelihood does not decrease at each step of the algorithm. Specifically, in the C-step, we sequentially update each column of $\mathbf{W}^{(t)}$, keeping all the other columns fixed, by maximizing the objective function under the constraint on the number of reliable cells per variable. Therefore, for each column we do not decrease the objective function and this guarantees that, eventually, $\ell(\widehat{\Psi}^{(t)}, \mathbf{W}^{(t+1)}; \mathbf{X}) \geq \ell(\widehat{\Psi}^{(t)}, \mathbf{W}^{(t)}; \mathbf{X})$. The other two steps correspond to the traditional E- and M-step of the EM algorithm with missing data (Ghahramani and Jordan, 1995) for which, given $\mathbf{W}^{(t+1)}$, the objective function does not decrease (see Little and Rubin, 2019, Section 11.3). The same holds for the penalized approach, where $\ell_{\text{pen}}(\widehat{\Psi}^{(t+1)}, \mathbf{W}^{(t+1)}; \mathbf{X}) \geq \ell_{\text{pen}}(\widehat{\Psi}^{(t)}, \mathbf{W}^{(t)}; \mathbf{X}), \forall t = 0, 1, 2, \dots$. \square

Algorithm 1 Initialization of \mathbf{W} (Step 1)

- 1: **Input:** \mathbf{X} , α_{tclust} , α_1 , α_2 , G
- 2: $p \leftarrow$ number of columns (variables) in \mathbf{X}
- Univariate TCLUST**
- 3: **for** $j_1 \leftarrow 1 : p$ **do**
- 4: $\text{tc}_1[[j_1]] \leftarrow \text{tclust}(\mathbf{X}[, j_1], \mathbf{k} = G, \mathbf{alpha} = \alpha_{\text{tclust}})$, where only observed units in variable j_1 are considered
- 5: **end for**
- 6: **for** $j_1 \leftarrow 1 : p$ **do**
- 7: $\text{MD}_1 \leftarrow$ compute MD for each unit per component according to the parameters obtained from univariate TCLUST
- 8: $\mathbf{f}_1[, j_1] \leftarrow$ select the minimum MD_1 across components
- 9: **end for**

Detection of cellwise outliers through univariate TCLUST

- 10: $\text{qq}_1 \leftarrow \text{quantile}(\mathbf{f}_1, 1 - \alpha_1, \mathbf{na.rm} = \text{TRUE})$
- 11: $\mathbf{W}_{(1)}[\mathbf{f}_1 > \text{qq}_1] \leftarrow 0$, where $\mathbf{W}_{(1)}$ has been initialized as $\mathbf{1}_n \mathbf{1}'_p$ (i.e., an $n \times p$ matrix of ones)

Bivariate TCLUST

- 12: **for** $j_1 \leftarrow 1 : (p - 1)$ **do**
- 13: **for** $j_2 \leftarrow (j_1 + 1) : p$ **do**
- 14: $\text{tc}_2[[j_1]][[j_2]] \leftarrow \text{tclust}(\text{cbind}(\mathbf{X}[, j_1], \mathbf{X}[, j_2]), \mathbf{k} = G, \mathbf{alpha} = \alpha_{\text{tclust}})$, where only observed units in both variables j_1 and j_2 are considered

```

15: end for

16: end for

17: for  $j_1 \leftarrow 1 : (p - 1)$  do

18:   for  $j_2 \leftarrow (j_1 + 1) : p$  do

19:      $\text{MD}_2 \leftarrow$  compute MD for each unit per component according to the parameters
      from bivariate TCLUST

20:      $f_2[, j_1, j_2] \leftarrow$  select the minimum  $\text{MD}_2$  across components

21:   end for

22: end for

```

Detection of cellwise outliers through bivariate TCLUST by excluding the already flagged cells

```

23: for  $j \leftarrow 1 : p$  do

24:    $f_2[\mathbf{W}_{(1)}[, j] == 0, j, ] \leftarrow \text{NA}$ 

25:    $f_2[\mathbf{W}_{(1)}[, j] == 0, , j] \leftarrow \text{NA}$ 

26: end for

27: for  $j \leftarrow 1 : p$  do

28:    $\text{ff}_2[, j] \leftarrow \text{apply}(f_2[, j, ], 1, \text{sum}, \text{na.rm} = \text{TRUE}) + \text{apply}(f_2[, , j], 1, \text{sum}, \text{na.rm} =$ 
       $\text{TRUE})$ 

29: end for

30:  $\text{ff}_2[\mathbf{W}_{(1)} == 0] \leftarrow \text{NA}$ 

31:  $\text{qq}_2 \leftarrow \text{quantile}(\text{ff}_2, 1 - \frac{\alpha_1}{1 - \alpha_2}, \text{na.rm} = \text{TRUE})$ 

```

32: $\mathbf{W}_{(2)}[\mathbf{f}\mathbf{f}_2 > \mathbf{q}\mathbf{q}_2] \leftarrow 0$, where $\mathbf{W}_{(2)}$ has been initialized as $\mathbf{1}_n \mathbf{1}'_p$ and NA values in $\mathbf{W}_{(2)}$

are replaced by 1

33: $\mathbf{W} \leftarrow \mathbf{W}_{(1)} \odot \mathbf{W}_{(2)}$ (Hadamard or element-wise product), where cells corresponding to NA values in \mathbf{X} are set to 0

34: **Output:** \mathbf{W}

The stopping criterion used for the cellGMM algorithm considers Aitken's acceleration procedure (Böhning et al., 1994; McLachlan and Peel, 2000, Section 2.11; McLachlan and Krishnan, 2008, Section 4.9). This is based on the Aitken-accelerated estimate of the log-likelihood – for simplicity, we denote hereinafter $\ell(\Psi, \mathbf{W}; \mathbf{X})$ as ℓ – which is defined at iteration $t + 1$ as

$$\ell_{\infty}^{(t+1)} = \ell^{(t)} + \frac{1}{1 + a^{(t)}} (\ell^{(t+1)} - \ell^{(t)}),$$

where $a^{(t)} = \frac{\ell^{(t+1)} - \ell^{(t)}}{\ell^{(t)} - \ell^{(t-1)}}$. The algorithm is considered to have converged if $\ell_{\infty}^{(t+1)} - \ell^{(t)} < \epsilon$ (McNicholas et al., 2010), where ϵ is an arbitrary small positive constant ($\epsilon = 10^{-6}$ in our experiments).

Algorithm 2 Step 2.2 of the initialization of Ψ

1: **Input:** $\mathbf{X}, G, \alpha_{A2}, n_{start}, n_{iter}, \mathbf{tclust}_\mu, \mathbf{tclust}_\Sigma$ (n_{iter} , \mathbf{tclust}_μ and \mathbf{tclust}_Σ come from Step 2.1)

2: **obj.best** $\leftarrow +\infty$

3: **for** $start \leftarrow 1 : n_{start}$ **do**

4: Sample one of the n_{rep} subsets of variables used for obtaining \mathbf{tclust}_μ and \mathbf{tclust}_Σ and initialize the centers of center groups in \mathbf{N} as the \mathbf{tclust}_μ corresponding to the selected repetition

5: **for** $iter \leftarrow 1 : n_{iter}$ **do**

6: Compute distances between the centers \mathbf{tclust}_μ and the centers of center groups in \mathbf{N}

7: Assign each center in \mathbf{tclust}_μ to the corresponding group $g \in \{1, \dots, G\}$ according to the minimum distance

8: Update the rows of \mathbf{N} as the mean of the corresponding centers in \mathbf{tclust}_μ assigned to the g th group, $g = 1, \dots, G$, by excluding a proportion α_{A2} of centers in \mathbf{tclust}_μ with the most “extreme” distances

9: **end for**

10: **obj** \leftarrow sum of distances across n_{rep} repetitions and G groups

11: **if** $\mathbf{obj} < \mathbf{obj}.best$ **then**

12: Update $\{\boldsymbol{\mu}_g\}_{g=1}^G$ and group assignment of the centers in \mathbf{tclust}_μ

13: $\mathbf{obj}.best \leftarrow \mathbf{obj}$

14: **end if**

15: **end for**

16: Compute $\{\Sigma_g\}_{g=1}^G$ as the mean of the covariance matrices in tclust_Σ according to the group assignment obtained for the centers in tclust_μ and check for the eigenvalue-ratio constraint

17: Compute the weights $\{\pi_g\}_{g=1}^G$ according to the minimum squared Euclidean distance of each observation from $\{\mu_g\}_{g=1}^G$

18: **Output:** initial parameters $\Psi = \{\pi, \theta\}$, where $\pi = \{\pi_g\}_{g=1}^G$ and $\theta = \{\mu_g, \Sigma_g\}_{g=1}^G$

2 Simulation study: additional results

We present herein the results of several additional simulation studies beyond those reported in Section 3 of the main article. These include three scenarios with less extreme cellwise outliers and missing data (Section 2.1) and three scenarios with more extreme contamination (Section 2.2). For all nine scenarios considered, we provide the number of samples on which each model can be properly computed in Table 1. In addition to the indices already introduced in Section 3 of the main article for assessing the models' performance, we report the Adjusted Rand Index (ARI, Hubert and Arabie, 1985), the Root Mean Squared Error of the posterior probabilities and the Mean Squared Error of the prior probabilities. These indices for Scenarios 1-3 are reported in Figure 1. Computation times for the methodologies implemented in Section 3 of the main article are reported in Section 2.5, along with the computational complexity of cellGMM. Finally, in Section 2.3, we present the results for Scenarios 1 and 2 with a higher percentage (20%) of both less and more extreme outlying values, while a simulation study in which cellGMM is applied to data sets contaminated by structurally outlying cells is illustrated in Section 2.4.

Table 1: Number of samples on which each model can be properly run per scenario, percentage of contamination, and model. Dashes represent scenarios where models cannot be implemented or where implementation is not necessary

% out.	Model	Less extreme outliers						More extreme outliers		
		Scenario 1	Scenario 2	Scenario 3	Scenario 4	Scenario 5	Scenario 6	Scenario 1	Scenario 2	Scenario 3
0	cellGMM.pen0	100	100	100	100	100	100	-	-	-
	cellGMM.penb	100	100	100	100	100	100	-	-	-
	TCLUST	100	100	100	-	-	-	-	-	-
	sclust_25	98	100	0	-	-	-	-	-	-
	MNM	100	100	100	100	100	100	-	-	-
	MCNM	100	100	100	80	78	13	-	-	-
	MtM	100	100	100	100	100	100	-	-	-
5	cellGMM.pen0	100	100	100	100	100	100	100	100	100
	cellGMM.penb	100	100	100	100	100	100	100	100	100
	TCLUST	100	100	100	-	-	-	100	100	100
	sclust_25	97	94	0	-	-	-	31	0	0
	sclust_5	93	90	90	-	-	-	22	0	3
	MNM	100	100	100	100	100	100	98	91	99
	MCNM	100	100	100	16	24	0	96	61	76
10	MtM	100	100	100	100	100	100	96	61	76
	cellGMM.pen0	100	100	100	100	100	100	100	100	100
	cellGMM.penb	100	100	100	100	100	99	100	100	100
	TCLUST	100	100	100	-	-	-	100	100	100
	sclust_25	93	88	0	-	-	-	3	0	0
	sclust_10	88	63	53	-	-	-	3	0	0
	MNM	100	100	100	100	100	100	100	100	76
15	MCNM	100	100	100	31	25	0	100	100	57
	MtM	100	100	100	100	100	99	100	100	62

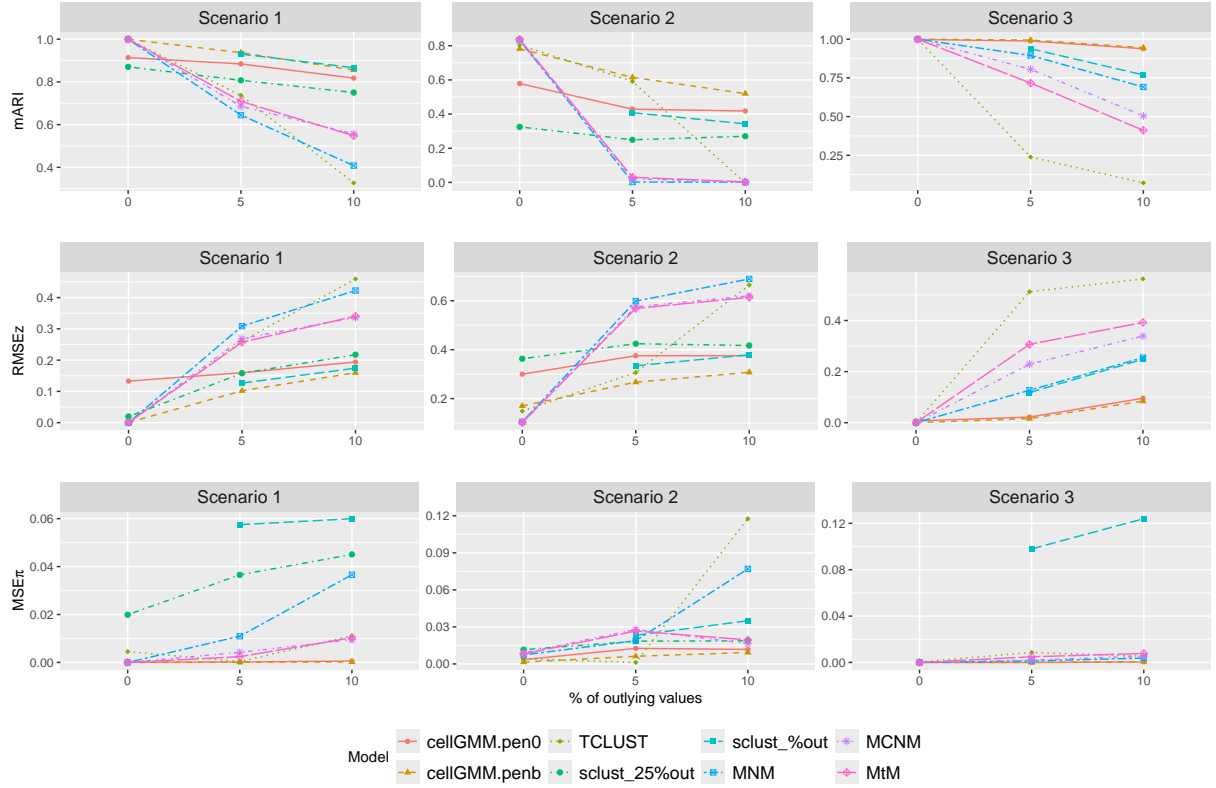


Figure 1: Results of the simulation study with less extreme outliers: mean of the Adjusted Rand Index (mARI), Root Mean Squared Error (RMSE) of the posterior probabilities and Mean Squared Error (MSE) of the prior probabilities per scenario, percentage of contamination, and model

2.1 Less extreme outliers

The three additional scenarios with less extreme outliers are as follows: *Scenario 4* and *Scenario 5* with $n = 200, p = 5, G = 2$, non-spherical with $\Sigma_1 = [\sigma_{ij} = 0.9^{|i-j|} : i, j = 1, \dots, p]$ and Σ_2 obtained by an orthogonal rotation of Σ_1 , unbalanced ($\pi = [0.3, 0.7]$) and well-separated and close components, respectively; *Scenario 6* with $n = 400, p = 15, G = 4$, non-spherical with $\Sigma_1 = \Sigma_2 = [\sigma_{ij} = 0.9^{|i-j|} : i, j = 1, \dots, p]$ and $\Sigma_3 = \Sigma_4$ obtained by an orthogonal rotation of Σ_1 , unbalanced ($\pi = [0.2, 0.2, 0.3, 0.3]$) and well-separated components. The component mean vectors are generated from uniform distributions. Specifically, $\mu_1 = \mathbf{0}$, and the elements of $\mu_g, g = 2, \dots, G$, are drawn from a uniform distribution in $[0, 10]$ in the well-separated case, and from $[1, 3]$ in the close case. In the former, we assess whether the distance between the component mean vectors is less than 5, and re-generate them if this occurs. The components' configuration is controlled through the overlapping measure ω introduced by Maitra and Melnykov (2010), where well-separated and close components correspond to $\omega_{\max} < 0.01$ and $0.05 < \omega_{\max} < 0.06$, respectively. For each scenario, we generate 100 data matrices that we contaminate with 0%, 5%, and 10% of outlying cells randomly drawn from a uniform distribution in the interval $[-10, 10]$, ensuring that the contaminated observations do not lie within the 99th percentile ellipsoid of any component. Moreover, we randomly remove 5% of the cells which have not been contaminated to obtain samples with missing data. Due to the latter, the only models we can compare to cellGMM are those included in the R package `MixtureMissing`, i.e., MNM, MCNM, MtM, since they can handle missing values.

The results of the classification performance and parameter estimates are reported in

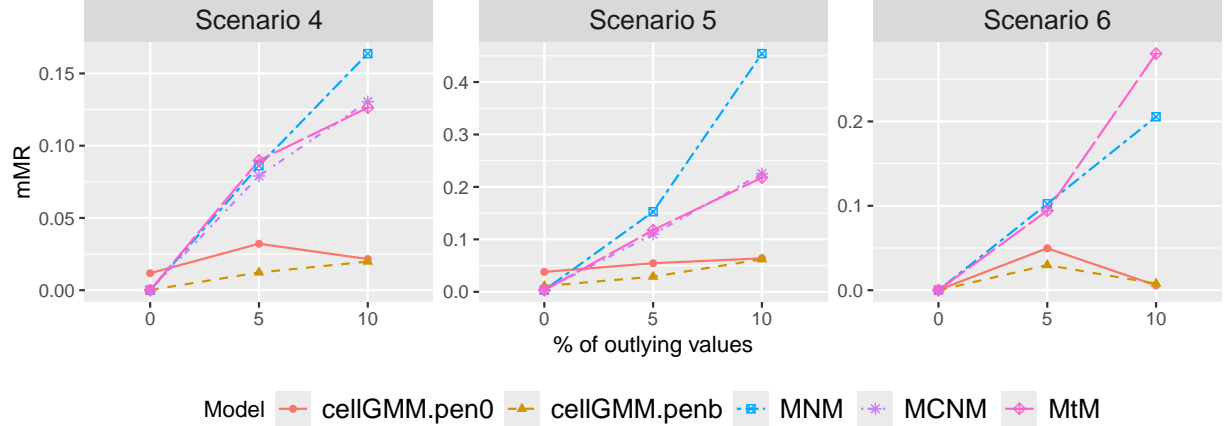


Figure 2: Results of the simulation study with less extreme outliers: mean of the Misclassification Rate (mMR) per scenario, percentage of contamination, and model

Figures 2, 3, and 4. As the level of contamination and the dimensionality of the data increase, the difference between cellGMM, specifically its penalized version (i.e. cellGMM.penb), and the competitors grows. Notably, in Scenario 6 with 10% of cellwise outliers, cellGMM.penb improves the parameter estimates compared to cellGMM.pen0, although this improvement is not reflected in the averaged ARI over the 100 samples. This is due to the distribution of the contaminated data being, by chance, well balanced among variables. In Table 2, we illustrate the results of the model on outlier detection and the corresponding value imputation for the aforementioned models, as well as cellMCD and DI. It should be noted that, unlike for Scenarios 1-3 analyzed in the main article, Table 2 shows non-null values of indices for the imputation evaluation of the model-based clustering competitors, referring only to the missing values. Dashes indicate cases where the models cannot be run on any sample because errors occur in the code. Overall, cellGMM.penb outperforms the competitors by balancing good performance on TP% and FP% and data

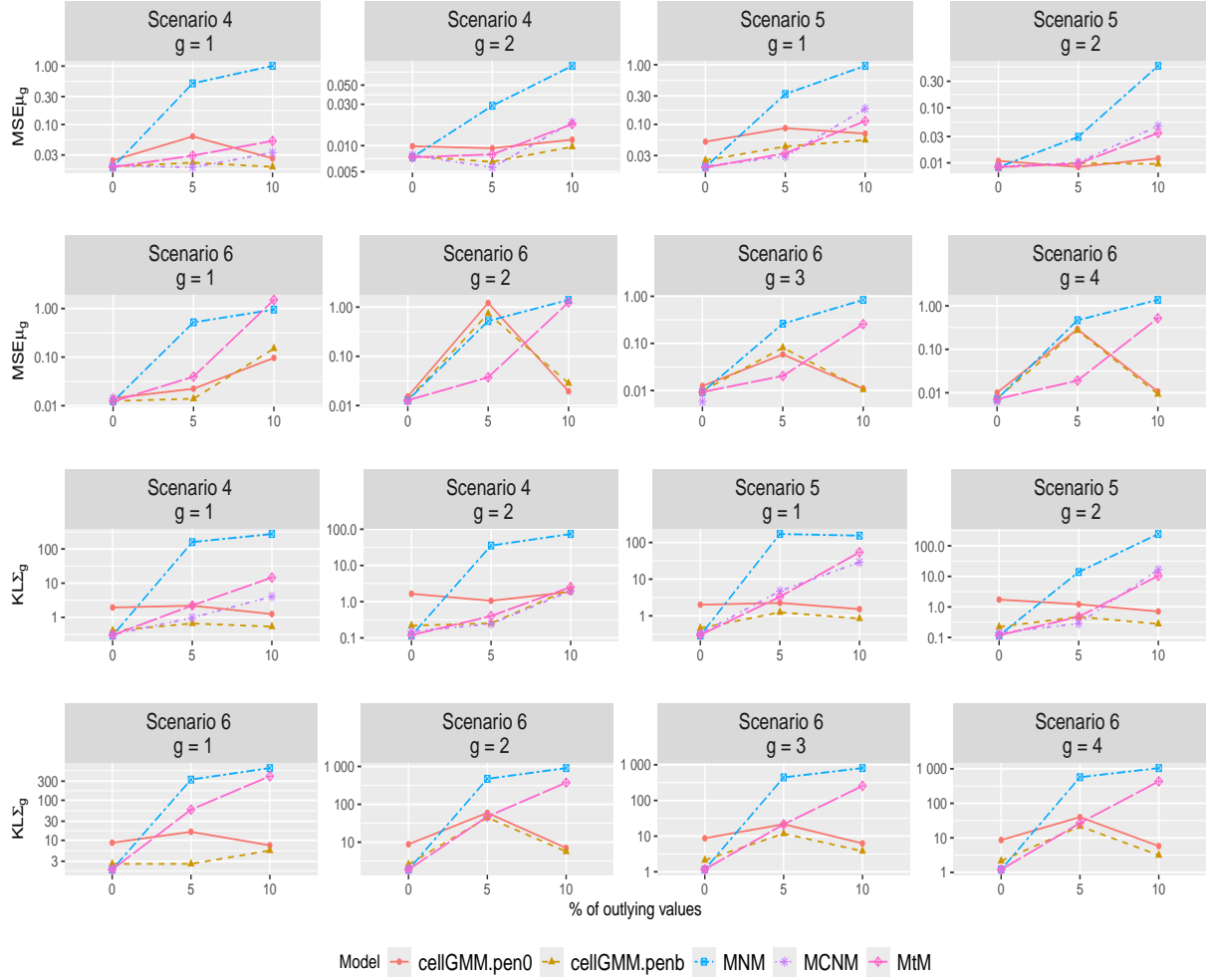


Figure 3: Results of the simulation study with less extreme outliers: Mean Squared Error (MSE) of the component mean vectors and Kullback-Leibler (KL) discrepancy for the component covariance matrices per scenario, percentage of contamination, and model. The values are represented via log-transformation, while the y-axis ticks are labeled using the original scale

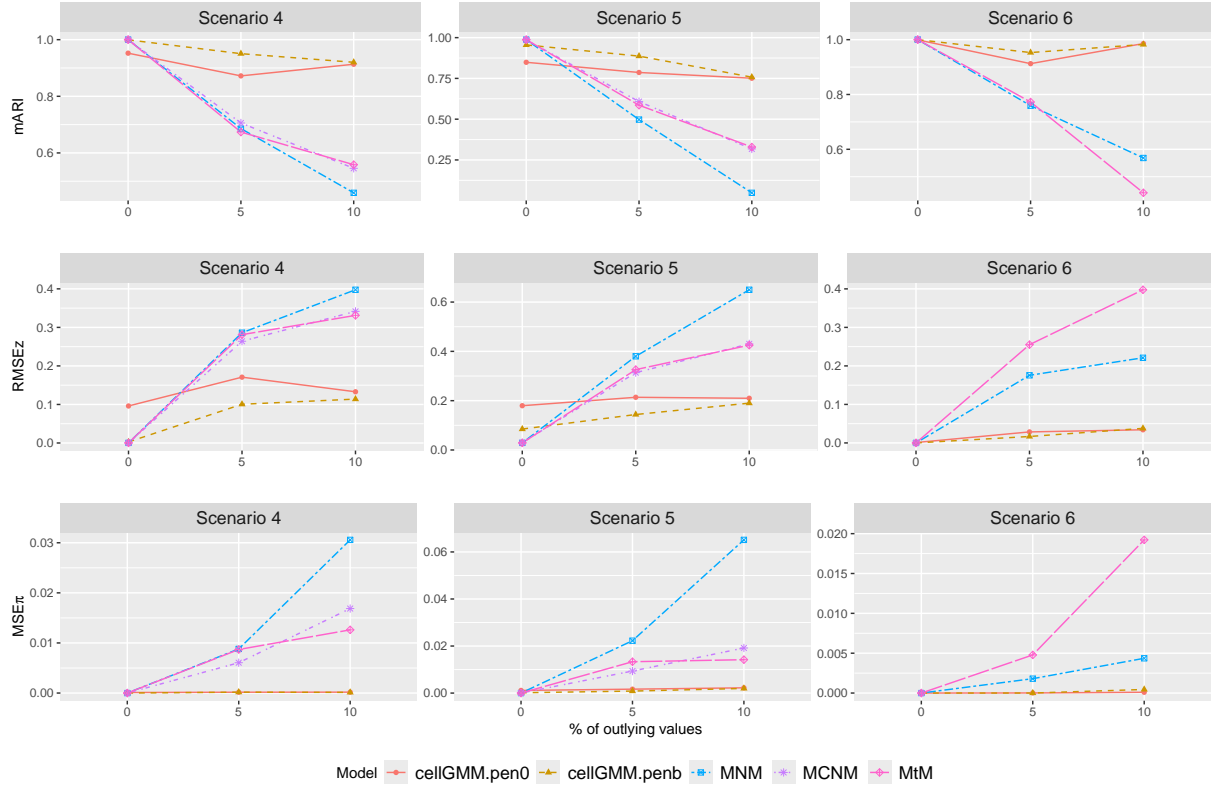


Figure 4: Results of the simulation study with less extreme outliers: mean of the Adjusted Rand Index (mARI), Root Mean Squared Error (RMSE) of the posterior probabilities and Mean Squared Error (MSE) of the prior probabilities per scenario, percentage of contamination, and model

Table 2: Outlier detection and imputation with less extreme outliers: percentage of True and False Positive (%TP and %FP), Mean Absolute and Root Mean Squared Error (MAE and RMSE) for comparing the original and imputed data matrices per scenario, percentage of contamination, and model

		Scenario 4				Scenario 5				Scenario 6			
% out.	Method	%TP	%FP	MAE	RMSE	%TP	%FP	MAE	RMSE	%TP	%FP	MAE	RMSE
0	cellGMM.pen0	-	19.63	0.24	0.65	-	19.67	0.24	0.60	-	20.00	0.19	0.45
	cellGMM.penb	-	2.16	0.04	0.20	-	2.41	0.05	0.23	-	2.63	0.04	0.19
	MNM	-	-	0.02	0.09	-	-	0.02	0.10	-	-	0.02	0.09
	MCNM	-	4.09	0.02	0.09	-	4.35	0.02	0.10	-	43.20	0.02	0.09
	MtM	-	22.76	0.02	0.09	-	22.67	0.02	0.10	-	19.88	0.02	0.09
	cellMCD	-	17.49	0.92	2.35	-	10.52	0.28	0.87	-	6.73	0.41	1.60
	DI	-	1.44	0.05	0.27	-	4.64	0.13	0.49	-	1.45	0.09	0.67
5	cellGMM.pen0	92.24	19.60	0.30	0.99	94.76	19.59	0.26	0.72	95.35	19.98	0.23	0.68
	cellGMM.penb	92.98	6.89	0.09	0.47	95.00	7.35	0.09	0.37	93.95	6.89	0.07	0.35
	MNM	-	-	0.70	1.14	-	-	0.64	0.94	-	-	0.95	1.54
	MCNM	94.12	20.51	0.69	1.38	92.42	20.41	0.62	1.10	-	-	-	-
	MtM	99.54	37.85	0.67	1.33	99.34	37.11	0.63	1.09	93.93	48.76	0.79	1.38
	cellMCD	90.04	20.54	0.92	2.33	91.68	13.88	0.30	0.89	89.35	9.08	0.31	1.29
	DI	70.45	4.82	0.16	0.90	74.04	5.58	0.16	0.83	43.23	3.25	0.30	1.46
10	cellGMM.pen0	94.50	19.55	0.25	0.80	94.68	19.61	0.22	0.66	94.03	20.00	0.19	0.54
	cellGMM.penb	93.50	12.09	0.17	0.71	94.50	13.09	0.14	0.51	92.72	12.95	0.12	0.46
	MNM	-	-	0.94	1.52	-	-	0.71	1.02	-	-	1.30	1.98
	MCNM	91.16	35.64	0.94	1.68	84.56	33.59	0.77	1.24	-	-	-	-
	MtM	97.84	46.95	0.88	1.66	91.82	44.90	0.74	1.19	79.41	54.32	1.06	1.69
	cellMCD	87.75	22.06	0.87	2.23	90.83	13.72	0.17	0.55	86.04	11.77	0.27	1.13
	DI	68.03	8.07	0.29	1.26	73.09	9.17	0.26	1.11	41.71	4.79	0.47	1.90

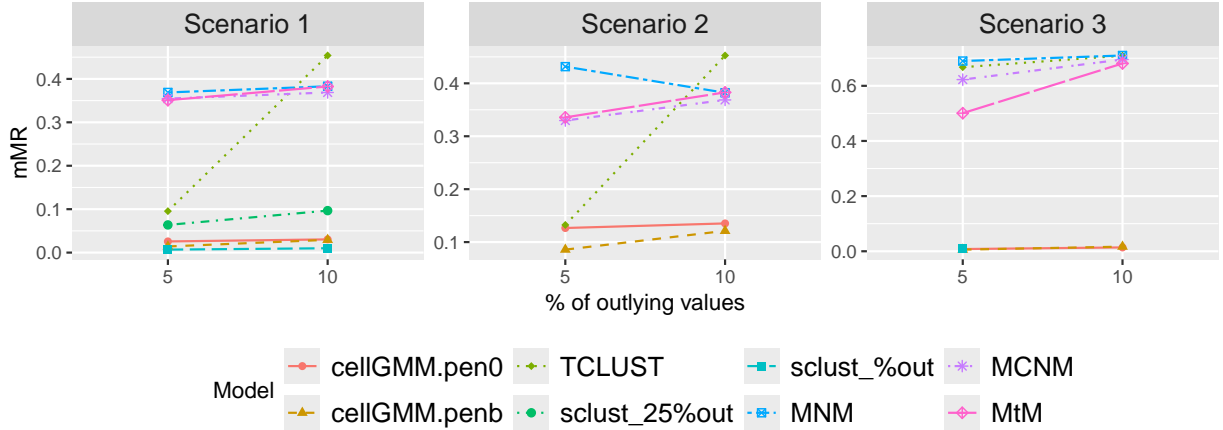


Figure 5: Results of the simulation study with more extreme outliers: mean of the Misclassification Rate (mMR) per scenario, percentage of contamination, and model imputation.

2.2 More extreme outliers

The last three scenarios replicate Scenarios 1-3 of the main article, with 5% and 10% of cell-wise outliers randomly drawn from a uniform distribution in the wider interval $[-100, 100]$ without any additional constraints. Looking at Figures 5, 6, and 7 and Table 3, it is evident that the model-based clustering methodologies with heavy-tailed distributions and non-robust GMM break down. Generally, we can deduce similar conclusions to the three scenarios reported in the main article, although those illustrated here demonstrate the advantage of cellGMM in handling more extreme outliers.

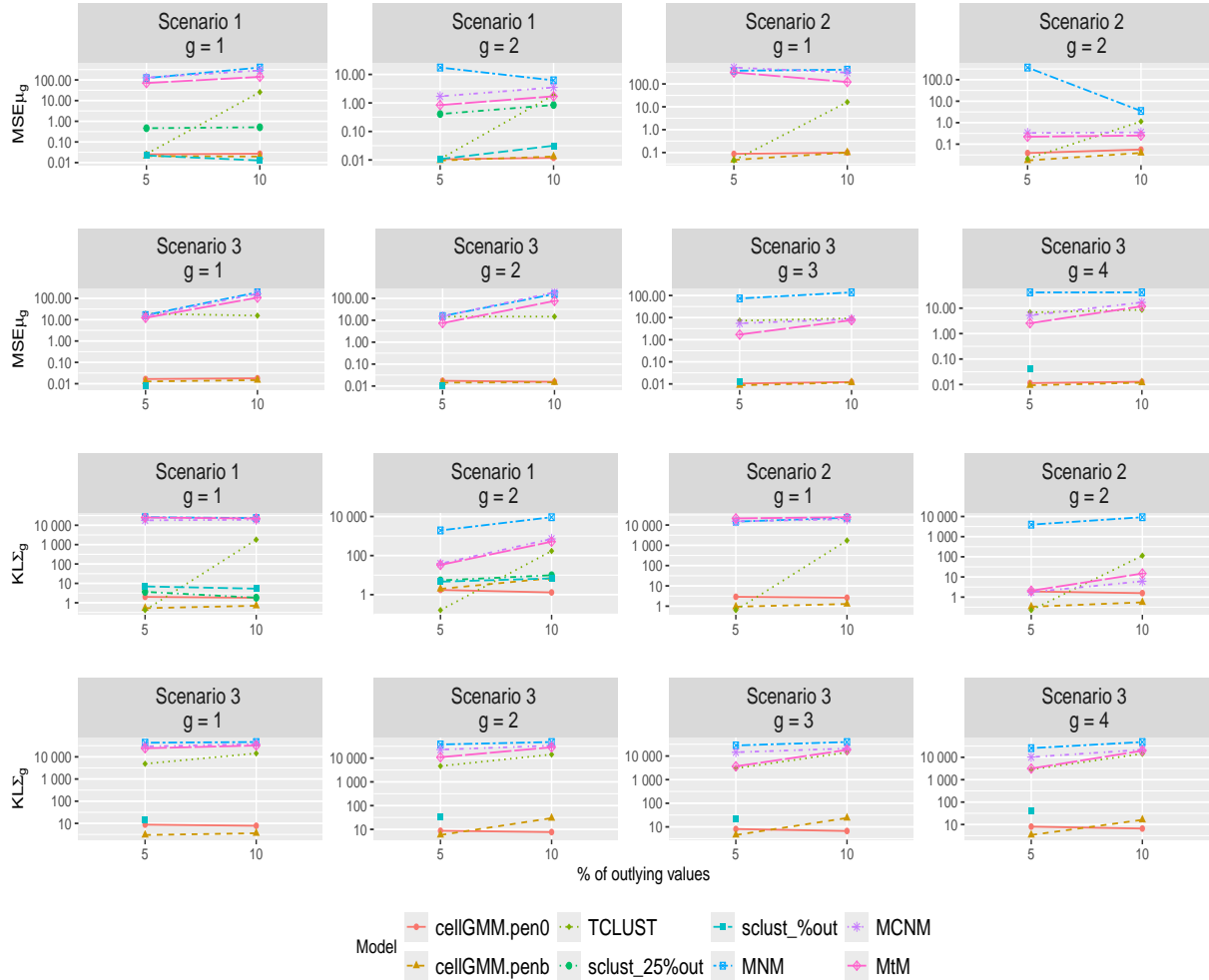


Figure 6: Results of the simulation study with more extreme outliers: Mean Squared Error (MSE) of the component mean vectors and Kullback-Leibler (KL) discrepancy for the component covariance matrices per scenario, percentage of contamination, and model. The values are represented via log-transformation, while the y-axis ticks are labeled using the original scale

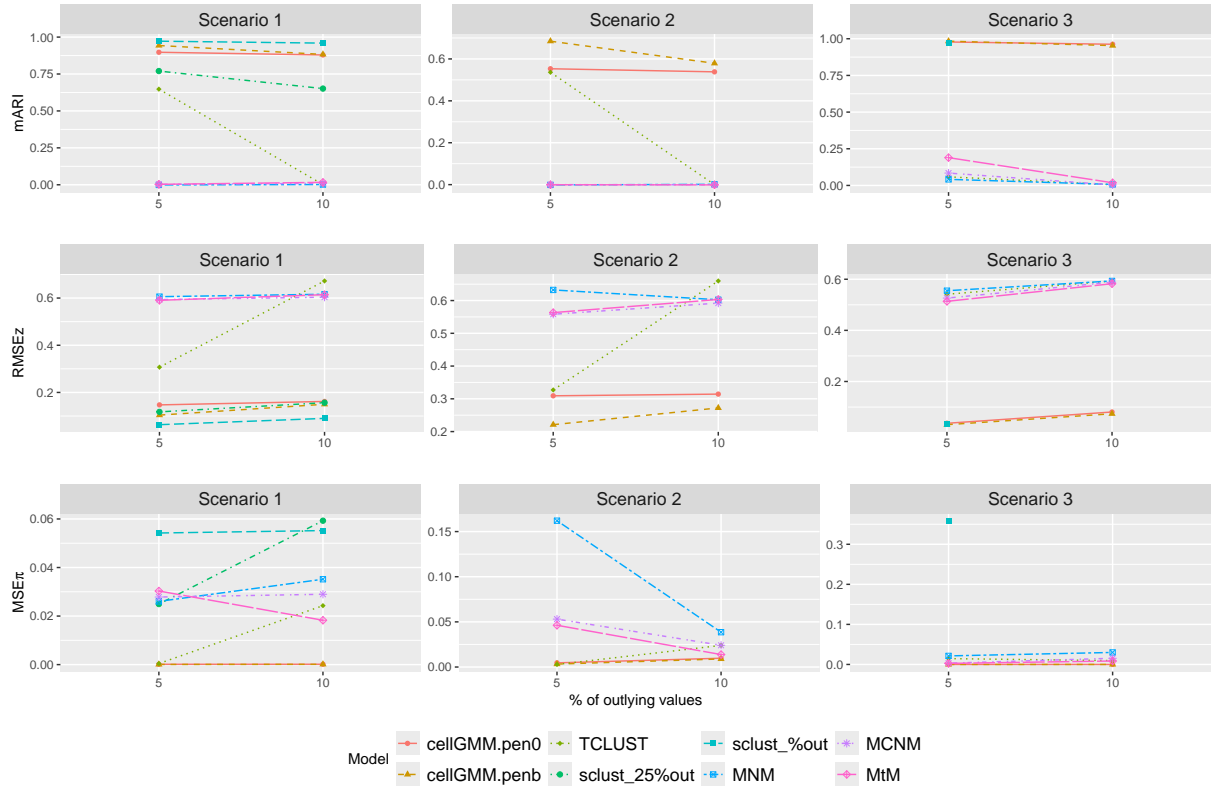


Figure 7: Results of the simulation study with more extreme outliers: mean of the Adjusted Rand Index (mARI), Root Mean Squared Error (RMSE) of the posterior probabilities and Mean Squared Error (MSE) of the prior probabilities per scenario, percentage of contamination, and model

Table 3: Outlier detection and imputation with more extreme outliers: percentage of True and False Positive (%TP and %FP), Mean Absolute and Root Mean Squared Error (MAE and RMSE) for comparing the original and imputed data matrices per scenario, percentage of contamination, and model

% out.	Method	Scenario 1				Scenario 2				Scenario 3			
		%TP	%FP	MAE	RMSE	%TP	%FP	MAE	RMSE	%TP	%FP	MAE	RMSE
5	cellGMM.pen0	98.92	21.11	0.22	0.58	98.86	21.11	0.20	0.48	99.37	21.09	0.23	0.61
	cellGMM.penb	98.94	3.92	0.10	0.53	98.76	5.05	0.10	0.43	99.16	4.24	0.08	0.41
	TCLUST	98.94	21.11	-	-	98.78	21.12	-	-	57.06	23.31	-	-
	sclust_25	96.65	21.23	-	-	-	-	-	-	-	-	-	-
	sclust_5	91.64	0.44	-	-	-	-	-	-	92.11	0.42	-	-
	MCNM	57.19	10.19	-	-	75.31	13.81	-	-	40.01	15.03	-	-
	MtM	63.83	37.28	-	-	72.72	34.10	-	-	79.59	40.78	-	-
	cellMCD	98.68	13.78	0.52	1.46	98.68	2.18	0.04	0.21	98.74	3.94	0.23	1.14
10	DI	98.36	3.83	0.12	0.43	98.62	1.91	0.04	0.21	98.72	8.12	0.37	1.28
	cellGMM.pen0	98.58	16.82	0.23	0.66	98.92	16.79	0.20	0.49	99.21	16.75	0.23	0.68
	cellGMM.penb	98.55	6.10	0.19	0.80	98.83	6.77	0.16	0.57	98.96	5.90	0.15	0.66
	TCLUST	65.86	20.46	-	-	65.84	20.46	-	-	47.54	22.50	-	-
	sclust_25	95.00	17.22	-	-	-	-	-	-	-	-	-	-
	sclust_10	93.00	0.78	-	-	-	-	-	-	-	-	-	-
	MCNM	70.77	22.93	-	-	70.96	23.04	-	-	47.14	25.09	-	-
	MtM	71.25	35.34	-	-	71.59	33.87	-	-	71.00	47.06	-	-
	cellMCD	98.72	13.41	0.53	1.47	98.82	1.96	0.06	0.24	98.61	2.84	0.18	0.93
	DI	98.06	1.60	0.07	0.27	98.84	1.92	0.06	0.24	98.72	2.57	0.12	0.57

2.3 Higher level of contamination

We present herein the results of the simulation study for Scenarios 1 and 2 with 20% of both less and more extreme outlying values. Tables 4 and 5 show that the performance of cellGMM deteriorates compared to scenarios with lower contamination levels, as expected. Indeed, 20% of outlying cells represents a very high level of contamination in the cellwise framework, undoing the potential of the proposal when more observations, variables, and clusters are considered, as in Scenario 3.

This analysis empirically assesses the robustness of cellGMM, in addition to the scenarios reported in Section 2.2. The breakdown properties of cellGMM may not be directly derived from those of cellMCD in the single-population framework. This is also the case for TCLUST, which extends MCD to heterogeneous populations, where the notion of breakdown points depend on non-trivial “cluster separation” assumptions (see Ruwet et al., 2013, for further details). An in-depth theoretical discussion of these properties for cellGMM will be provided in future work.

2.4 Structural outlier generation

In the simulation studies presented so far, we have considered random contamination affecting a certain percentage of the $n \times p$ cells in a data matrix. In this section, we also explore the performance of cellGMM in the presence of structural outliers. We focus on Scenarios 1 and 2 previously illustrated, where the prior probabilities are set to $\pi = [0.7, 0.3]$. We replace 5%, 10%, and 20% of the cells in the submatrix corresponding to the observations generated from the first component with contaminated values, extending the generation

Table 4: Classification and parameter estimation results for the simulation study with 20% of contamination per scenario, outlying value generation, and model

Outliers	Model	# samp.	mARI	mMR	RMSE _{π}	MSE _{π}	MSE _{μ_1}	MSE _{μ_2}	KL _{Σ_1}	KL _{Σ_2}
Scenario 1										
Less extreme	cellGMM.pen0	100	0.85	0.04	0.19	0.00	0.09	0.02	0.96	0.72
	cellGMM.penb	96	0.71	0.08	0.25	0.01	0.57	0.05	1.91	4.66
	TCLUST	100	0.08	0.38	0.60	0.06	3.90	1.49	195.39	152.50
	sclust_25	63	0.73	0.07	0.25	0.05	0.66	0.61	39.15	26.31
	sclust_20	66	0.76	0.06	0.24	0.06	0.44	0.37	46.65	27.19
	MNM	100	0.22	0.27	0.51	0.08	1.32	0.28	410.90	181.13
	MCNM	100	0.19	0.28	0.51	0.03	0.97	0.05	133.85	17.65
More extreme	MtM	100	0.18	0.29	0.52	0.04	1.03	0.08	184.67	45.86
	cellGMM.pen0	98	0.90	0.03	0.14	0.00	5.89	0.02	1.45	0.87
	cellGMM.penb	24	0.88	0.03	0.15	0.00	0.03	0.01	0.57	3.78
	TCLUST	100	0.00	0.50	0.70	0.08	15.63	23.81	5975.82	9165.80
	sclust_25	1	0.92	0.02	0.14	0.00	0.04	0.09	4.63	11.00
	sclust_20	0	-	-	-	-	-	-	-	-
	MNM	100	0.00	0.41	0.63	0.05	572.85	11.86	20993.78	28767.40
More extreme	MCNM	100	0.00	0.43	0.65	0.02	37.96	3.57	26589.25	2464.01
	MtM	100	0.00	0.46	0.67	0.04	16.41	7.29	15076.11	10341.98
Scenario 2										
Less extreme	cellGMM.pen0	100	0.44	0.17	0.35	0.01	0.09	0.07	1.99	0.81
	cellGMM.penb	100	0.43	0.18	0.34	0.01	0.18	0.05	1.76	0.62
	TCLUST	100	0.00	0.49	0.67	0.07	1.07	0.64	96.62	199.22
	sclust_25	70	0.28	0.24	0.41	0.03	0.18	0.12	7.92	5.41
	sclust_20	51	0.31	0.22	0.40	0.04	0.20	0.09	9.84	6.87
	MNM	100	0.00	0.50	0.68	0.04	1.81	1.03	103.24	436.66
	MCNM	100	0.01	0.45	0.64	0.03	1.10	0.50	238.58	112.21
More extreme	MtM	100	0.01	0.44	0.63	0.02	0.89	0.33	262.47	105.37
	cellGMM.pen0	99	0.54	0.13	0.30	0.01	1.42	0.06	2.90	0.83
	cellGMM.penb	23	0.65	0.09	0.23	0.00	0.03	0.01	0.97	0.34
	TCLUST	100	0.00	0.49	0.69	0.07	10.36	20.71	5438.39	8969.34
	sclust_25	0	-	-	-	-	-	-	-	-
	sclust_20	0	-	-	-	-	-	-	-	-
	MNM	0	-	-	-	-	-	-	-	-
More extreme	MCNM	100	0.00	0.43	0.64	0.02	84.52	1.94	24365.74	1997.77
	MtM	100	0.00	0.46	0.66	0.04	10.91	5.04	15968.84	8942.05

Table 5: Outlier detection and imputation with 20% of contamination per scenario, outlying value generation, and model

Outliers	Method	Scenario 1				Scenario 2			
		%TP	%FP	MAE	RMSE	%TP	%FP	MAE	RMSE
Less extreme	cellGMM.pen0	91.36	8.41	0.26	0.89	92.47	8.13	0.19	0.56
	cellGMM.penb	88.01	5.46	0.31	1.09	91.33	4.64	0.18	0.56
	TCLUST	46.24	19.69	-	-	47.31	19.42	-	-
	sclust_25	65.47	14.88	-	-	83.88	10.28	-	-
	sclust_20	61.53	9.62	-	-	79.33	5.17	-	-
	MCNM	74.44	39.76	-	-	48.28	23.83	-	-
	MtM	77.70	43.84	-	-	63.50	36.41	-	-
	cellMCD	87.38	9.57	0.51	1.43	90.53	1.59	0.12	0.38
More extreme	DI	83.94	2.22	0.19	0.67	90.77	1.96	0.12	0.39
	cellGMM.pen0	98.52	6.62	0.18	0.68	98.67	6.58	0.15	0.42
	cellGMM.penb	98.27	3.52	0.18	0.73	98.50	3.38	0.14	0.48
	TCLUST	48.85	19.04	-	-	49.02	18.99	-	-
	sclust_25	95.50	7.38	-	-	-	-	-	-
	sclust_20	-	-	-	-	-	-	-	-
	MCNM	69.36	34.69	-	-	67.94	33.67	-	-
	MtM	72.03	41.24	-	-	71.86	39.79	-	-
	cellMCD	98.39	8.70	0.43	1.26	98.75	1.60	0.10	0.29
	DI	98.06	1.39	0.12	0.39	98.70	1.96	0.11	0.33

scheme of Raymaekers and Rousseeuw (2023) to the heterogeneous population framework.

Therefore, for each column of the data matrix, we randomly draw 5%, 10% or 20% of the indices to contaminate. The variables corrupted for each observation of the first component are stored into the set $K = \{j_1, \dots, j_k\}$, where $k = |K|$. It is worth noting that the contamination level is the same across variables but can differ for each unit. The k -dimensional vector of contaminated cells per observation is obtained as $-\gamma\sqrt{k}\frac{\nu_K}{\text{MD}(\nu_K, \mu_{1[K]}, \Sigma_{1[K]})}$, where γ quantifies the distance of the outlying cells from the center of the first component. Here, $\mu_{1[K]}$ and $\Sigma_{1[K]}$ denote the mean vector and the covariance matrix of the first component, respectively, restricted to the variables in K , and ν_K is the normed eigenvector of $\Sigma_{1[K]}$ corresponding to its largest eigenvalue. We vary γ in $\{1, 5, 10\}$. This generation scheme ensures that the resulting contaminated cells are structurally outlying in the corresponding subspace.

The results of this simulation study are reported in Tables 6 and 7. As γ increases, the classification performance of cellGMM.penb likely improves. Indeed, when $\gamma = 1$, several contaminated observations lie within the 99th percentile ellipsoid of one component, as reported in Table 8, making them hard to detect (see %TP in Tables 6 and 7). As discussed in the previous section, a 20% of contamination is very high and may limit the potential of the proposed methodology. This is particularly evident in Scenario 2 with close components, especially when $\gamma = 1$ where the level of contamination is underestimated by cellGMM.penb. In all other cases, the results presented here provide evidence of the potential of cellGMM in detecting structural outlying values.

Table 6: Results of the simulation study in the presence of structural outlying cells per percentage of contamination and γ level, for Scenario 1

% out.	γ	Model	# samp.	mMR	MSE_{μ_1}	MSE_{μ_2}	KL_{Σ_1}	KL_{Σ_2}	%TP	%FP
1	1	cellGMM.pen0	100	0.03	0.02	0.03	1.83	2.14	66.90	22.79
		cellGMM.penb	100	0.02	0.01	0.03	0.27	1.74	52.34	4.85
	5	cellGMM.pen0	100	0.03	0.01	0.02	1.74	1.84	99.26	21.09
		cellGMM.penb	100	0.01	0.01	0.02	0.29	2.32	100.00	4.21
5	10	cellGMM.pen0	100	0.03	0.01	0.02	1.76	1.87	99.84	21.06
		cellGMM.penb	100	0.02	0.01	0.02	0.30	3.00	100.00	4.73
	10	cellGMM.pen0	100	0.04	0.02	0.09	1.49	2.09	59.98	21.11
		cellGMM.penb	100	0.06	0.02	0.10	0.33	6.56	48.83	8.10
10	5	cellGMM.pen0	100	0.03	0.02	0.03	1.32	1.40	98.38	16.85
		cellGMM.penb	100	0.02	0.01	0.02	0.37	5.50	99.98	5.85
	10	cellGMM.pen0	100	0.03	0.01	0.02	1.35	1.44	99.61	16.71
		cellGMM.penb	100	0.03	0.01	0.03	0.38	6.60	100.00	6.64
20	1	cellGMM.pen0	100	0.06	0.07	0.87	1.90	2.92	41.51	20.87
		cellGMM.penb	100	0.16	0.09	2.50	2.80	27.29	24.99	15.76
	5	cellGMM.pen0	100	0.04	0.04	0.26	0.88	0.63	96.52	7.12
		cellGMM.penb	100	0.03	0.08	0.46	2.49	5.12	99.11	3.54
20	10	cellGMM.pen0	100	0.02	0.04	0.22	1.25	1.23	99.45	6.39
		cellGMM.penb	97	0.03	0.05	0.45	0.89	2.72	100.00	3.23

Table 7: Results of the simulation study in the presence of structural outlying cells per percentage of contamination and γ level, for Scenario 2

% out.	γ	Model	# samp.	mMR	MSE_{μ_1}	MSE_{μ_2}	KL_{Σ_1}	KL_{Σ_2}	%TP	%FP
5	1	cellGMM.pen0	100	0.14	0.08	0.08	2.15	2.87	66.52	22.81
		cellGMM.penb	100	0.11	0.06	0.09	0.45	1.05	53.42	6.07
	5	cellGMM.pen0	100	0.13	0.05	0.07	2.01	2.41	99.96	21.05
		cellGMM.penb	100	0.09	0.03	0.07	0.44	0.87	100.00	5.28
10	10	cellGMM.pen0	100	0.13	0.04	0.07	2.05	2.37	99.96	21.05
		cellGMM.penb	100	0.09	0.02	0.06	0.43	0.85	100.00	5.55
	5	cellGMM.pen0	100	0.19	0.16	0.21	1.94	2.84	57.22	21.42
		cellGMM.penb	100	0.21	0.18	0.30	0.77	1.87	47.02	9.06
20	5	cellGMM.pen0	100	0.13	0.04	0.06	1.62	2.01	99.97	16.67
		cellGMM.penb	100	0.12	0.03	0.08	0.56	1.04	100.00	6.68
	10	cellGMM.pen0	100	0.13	0.05	0.77	1.61	2.00	99.90	16.68
		cellGMM.penb	100	0.13	0.03	0.09	0.59	1.12	100.00	7.31
50	1	cellGMM.pen0	100	0.29	0.63	0.47	2.34	2.50	37.74	21.81
		cellGMM.penb	100	0.34	0.60	0.86	2.58	3.02	31.24	12.81
	5	cellGMM.pen0	100	0.09	0.02	0.47	0.78	0.87	99.73	6.32
		cellGMM.penb	100	0.10	0.03	0.09	0.54	0.60	100.00	3.50
100	10	cellGMM.pen0	100	0.15	0.11	19.58	1.01	1.73	99.80	6.30
		cellGMM.penb	100	0.10	0.04	0.09	0.58	0.82	100.00	3.56

Table 8: Percentage of contaminated observations that lie within the 99th percentile ellipsoid of one component averaged over 100 samples (# out. in), and level of contamination estimated by cellGMM.penb (Est. cont.) averaged over the number of samples on which the model can be properly computed per scenario, percentage of contamination, and γ level

		% out.	5%			10%			20%			
			γ	1	5	10	1	5	10	1	5	10
Scenario 1	# out. in	56.92	0.00	0.00	53.10	0.00	0.00	46.23	0.00	0.00		
	Est. cont.	7.23	9.00	9.49	12.18	15.27	15.98	17.60	22.66	22.58		
Scenario 2	# out. in	58.58	0.00	0.00	55.97	0.00	0.00	49.22	0.00	0.00		
	Est. cont.	8.44	10.02	10.27	12.86	16.02	16.58	16.50	22.80	22.85		

2.5 Computational aspects

In this section, we provide indicative information on the computation time of the cellGMM algorithm compared to the other methodologies implemented in the simulation study for the three scenarios illustrated in the main article. The computation times reported in Table 9 are obtained using a MacBook Pro with a 6-Core Intel Core i7 (2.6 GHz) processor and 16GB DDR4 RAM (2667 MHz). The runtime is averaged over 10 samples per scenario and percentage of contamination, for which all models have been properly implemented.

Table 9 shows that our proposal is more time-consuming compared to the other methodologies. This difference increases significantly with the dimensionality of the data. Nonetheless, a higher computational cost often corresponds to better results in terms of classification, parameter estimation, and outlier detection, as illustrated in Section 3 of the main article. The greatest runtime is required for the update of \mathbf{W} . Algorithmic optimization,

Table 9: Computation time in seconds averaged over 10 samples per scenario with different percentages of contamination and models. Dashes represent scenarios where models cannot be implemented or where implementation is not necessary

Model	0% out.			5% out.			10% out.		
	Scenario 1	Scenario 2	Scenario 3	Scenario 1	Scenario 2	Scenario 3	Scenario 1	Scenario 2	Scenario 3
cellGMM.pen0	11.82	19.81	339.33	13.80	20.13	372.76	15.19	24.42	410.48
cellGMM.penb	1.07	4.36	36.89	2.21	9.05	59.91	4.41	16.22	126.34
TCLUST	0.03	0.03	0.56	0.02	0.03	0.44	0.02	0.03	0.48
sclust_25	0.43	0.51	-	0.35	0.38	-	0.65	1.11	-
sclust_5	-	-	-	0.44	1.00	2.14	-	-	-
sclust_10	-	-	-	-	-	-	0.32	1.46	2.35
MNM	0.01	0.29	0.20	0.10	0.06	1.03	0.11	0.09	1.81
MCNM	2.06	2.55	16.88	0.38	1.15	5.21	0.48	0.99	7.44
MtM	2.05	2.06	10.63	0.35	1.37	9.31	0.42	1.94	14.41

which may include the use of a compiled programming language, is part of future developments. It is worth noting that if the user has prior information to set the penalty term in advance, cellGMM.penb can be run directly, thus speeding up the computation time.

The computational complexity of cellGMM is $\mathcal{O}(n \log(n)p + nGp^2)$. Specifically, the C-step costs $\mathcal{O}(n \log(n))$ for each variable to sort $\{\Delta_{ij}\}_{i=1}^n$ (Knuth, 1998). The computations in the E- and M-steps, which are also involved in the C-step, include the SWEEP operator, whose complexity $\mathcal{O}(nGp^2)$ (Goodnight, 1979) dominates both the covariance matrix inversion and the eigenvalue-ratio constraint. The latter have complexity $\mathcal{O}(Gp^3)$ (Grötschel et al., 1993) and $\mathcal{O}(G^2p^2)$, respectively, and the dominance holds since $n > G$ and $n > p$.

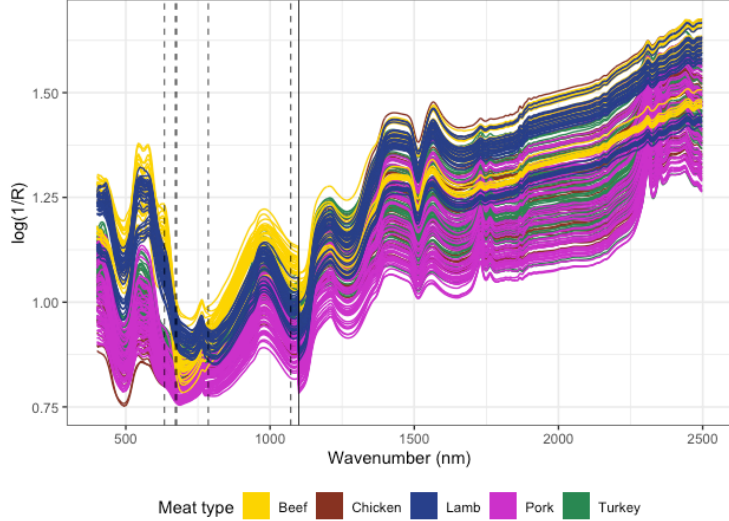


Figure 8: Homogenized Meat data set: visible and near infrared spectra of five homogenized meat types (dashed lines: selected wavelengths; solid line: discontinuity).

3 Real data examples: additional results

In this section, we provide additional results on the application of cellGMM to the real data sets illustrated in the main article.

3.1 Homogenized Meat Data Set

Near-infrared reflectance spectroscopy is a method often used for collecting data in food authenticity studies (Downey, 1996, among others) since it is able to discern the properties and, therefore, the nature of food samples. For each of the 231 homogenized meat samples 1050 reflectance measurements are collected with wavelengths between 400 nm and 2500 nm at 2 nm intervals (Figure 8). Due to the number of measurements, one of the first tasks to handle is to reduce the dimensionality of the data. Methods for variable selection were

Table 10: Adjusted Rand Index comparing the theoretical and the estimated classification of meat samples in two classes per model, and percentage of contamination and missing values, i.e. $(a\%, b\%)$

	cellGMM	TCLUST	sclust	MNM	MCNM	MtM
(0%, 0%)	0.95	1.00	1.00	1.00	1.00	1.00
(3%, 0%)	0.95	0.86	0.85	0.81	0.80	0.75
(3%, 2%)	0.95	-	-	0.80	0.78	0.75
(10%, 0%)	0.93	0.45	0.73	0.48	0.25	0.36

Table 11: Average cellGMM classification results of the meat species with $G = 3, 4, 5$ (3% of contamination)

	1	2	3		1	2	3	4		1	2	3	4	5
Beef	0.88	0.03	0.09	Beef	0.97	0.00	0.00	0.03	Beef	0.97	0.03	0.00	0.00	0.00
Lamb	0.06	0.91	0.03	Lamb	0.06	0.94	0.00	0.00	Lamb	0.12	0.88	0.00	0.00	0.00
				Pork	0.00	0.00	0.82	0.18	Pork	0.13	0.00	0.78	0.04	0.05
White meats	0.01	0.00	0.99	Poultry	0.01	0.00	0.15	0.84	Chicken	0.21	0.00	0.02	0.75	0.02
									Turkey	0.05	0.00	0.00	0.85	0.10

applied on this data set by Murphy et al. (2010) and, in a robust framework, by Cappozzo et al. (2021). We refer to the latter by considering five relevant wavelengths which span the protein spectral region.

As for the simulation study, we report herein the ARI between the theoretical and the estimated clustering structure for cellGMM and the other competitors. From Table 10, it is evident that as the level of contamination increases, the performance of the rowwise and non-robust model-based clustering competitors dramatically decreases, whereas that

of cellGMM diminishes less, remaining good. Additionally, Table 11 depicts the average classification results for cellGMM (i.e. cellGMM.penb) when $G = 3$, i.e., pork, chicken and turkey are merged together representing white meats, $G = 4$, i.e., chicken and turkey meats are considered in the same group representing poultry, and $G = 5$, all in the case of 3% of contamination. Although G is also set to 5, most of the chicken and turkey meats are grouped together, while the estimated cluster 5 contains few observations that are residual from the other clusters. The structure in four groups better distinguishes between the meat species, even if there is an “overlapping” between pork and poultry meats, while the classification in three clusters discriminates well among beef, lamb and white meats.

3.2 Top Gear Data Set

The scatterplot for pairs of variables referring to the original, potentially contaminated data with the estimated classification in four groups is reported in Figure 9, while the full list of four clusters’ classification is detailed below.

Cluster 1. Alfa Romeo Giulietta, Audi A3, Audi A4, Audi A4 Allroad, Audi A5, Audi A5 Sportback, Audi A6 Avant, Audi A6 Saloon, Audi Q3, Audi Q5, Audi TT Coupé, Audi TT Roadster, BMW 1 Series, BMW 1 Series Convertible, BMW 1 Series Coupé, BMW 3 Series, BMW 3 Series Convertible, BMW 4 Series Coupé, BMW i3, BMW X1, BMW Z4, Caterham CSR, Caterham Super 7, Chevrolet Cruze, Chevrolet Orlando, Chevrolet Volt, Chrysler Delta, Citroen C4, Citroen C4 Picasso, Citroen C5, Citroen DS3, Citroen DS4, Citroen DS5, Dacia Duster, Fiat Bravo, Fiat Doblò, Fiat Punto Evo, Ford C-Max, Ford Focus, Ford Focus Estate, Ford Focus ST, Ford Kuga,

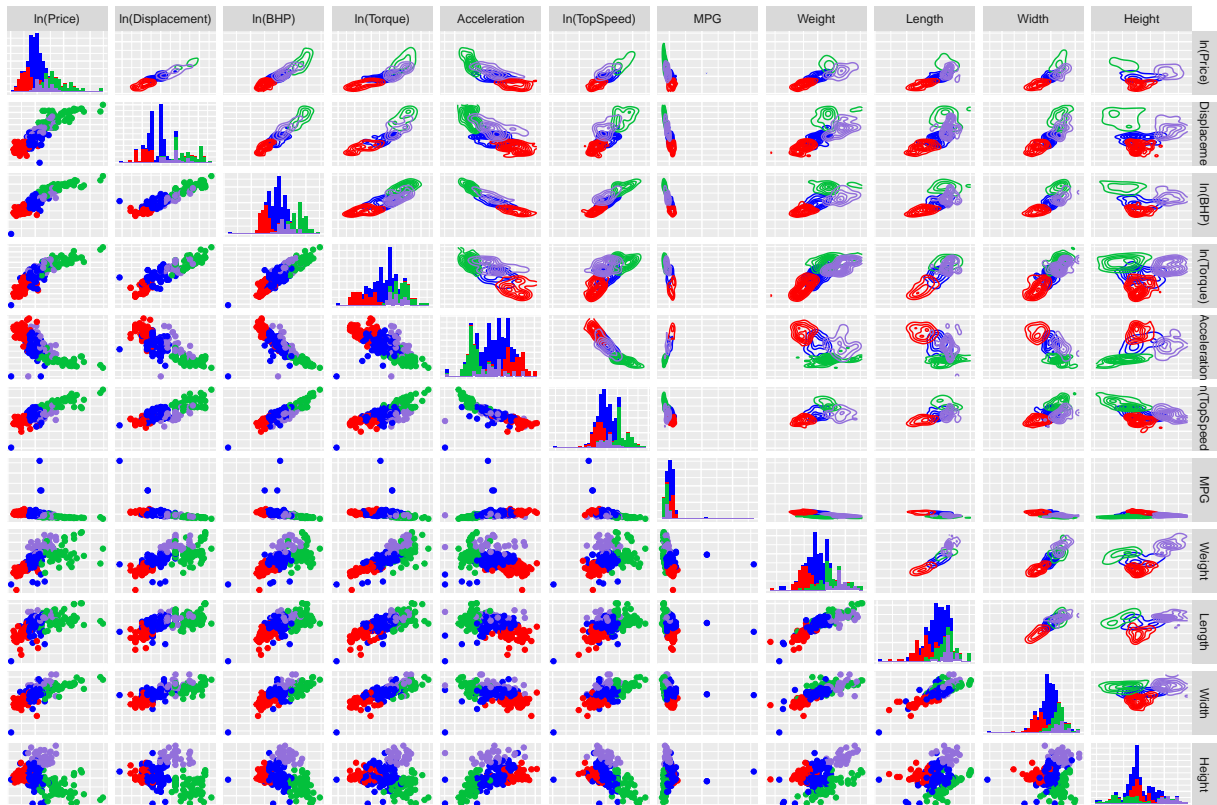


Figure 9: Pair plots of the Top Gear data set with the estimated classification in four groups (Cluster 1: blue; Cluster 2: red; Cluster 3: green; Cluster 4: purple)

Ford S-MAX, Honda Accord, Honda Civic, Honda CR-V, Honda CR-Z, Hyundai i40, Hyundai ix35, Hyundai Veloster, Jaguar XF, Jaguar XF Sportbrake, Jeep Compass, Kia Cee'd, Kia Optima, Kia Soul, Kia Sportage, Land Rover Freelander 2, Land Rover Range Rover Evoque, Lexus CT 200h, Lexus GS, Lotus Elise, Mazda CX-5, Mazda Mazda3, Mazda MX-5, Mercedes-Benz A-Class, Mercedes-Benz B-Class, Mercedes-Benz C-Class, Mercedes-Benz CLS Shooting Brake, Mercedes-Benz E-Class, Mercedes-Benz E-Class Coupé, Mercedes-Benz SLK, Mini Countryman, Mini Cooper, Mini John Cooper Works, Mini Roadster, Mitsubishi ASX, Mitsubishi Outlander, Morgan 3 Wheeler, Nissan Juke, Nissan Leaf, Nissan Qashqai, Nissan X-Trail, Peugeot 207 CC, Peugeot 3008, Peugeot 308, Peugeot 308 CC, Peugeot 308 SW, Peugeot 5008, Peugeot RCZ, Renault Mégane, Renault Scénic/Grand Scénic, Renault Twizy, SEAT Altea, SEAT León, Skoda Octavia, Skoda Yeti, Subaru BRZ, Subaru Forester, Subaru Legacy Outback, Subaru XV, Suzuki Grand Vitara, Toyota Avensis, Toyota GT 86, Toyota Prius, Toyota RAV4, Toyota Verso, Vauxhall Ampera, Vauxhall Astra, Vauxhall Astra GTC, Vauxhall Astra VXR, Vauxhall Cascada, Vauxhall Corsa VXR, Vauxhall Insignia, Vauxhall Insignia Sports Tourer, Vauxhall Mokka, Vauxhall Zafira, Vauxhall Zafira Tourer, Volkswagen Beetle, Volkswagen CC, Volkswagen Eos, Volkswagen Golf, Volkswagen Golf Plus, Volkswagen Jetta, Volkswagen Passat, Volkswagen Scirocco, Volkswagen Tiguan, Volkswagen Touran, Volvo S60, Volvo S80, Volvo V40, Volvo V60, Volvo V70, Volvo XC70.

Cluster 2. Alfa Romeo MiTo, Aston Martin Cygnet, Audi A1, Chevrolet Aveo, Chevrolet Spark, Chrysler Ypsilon, Citroen C1, Citroen C3, Citroen C3 Picasso, Dacia Sandero, Fiat

500, Fiat 500 Abarth, Fiat 500L, Fiat Panda, Ford B-Max, Ford Fiesta, Honda Insight, Honda Jazz, Hyundai i10, Hyundai i20, Hyundai i30, Hyundai ix20, Kia Picanto, Kia Rio, Kia Venga, Mini Clubman, Mini Convertible, Mitsubishi i-MiEV, Mitsubishi Mirage, Nissan Micra, Nissan Note, Perodua MYVI, Peugeot 107, Peugeot 207 SW, Peugeot 208, Proton GEN-2, Proton Satria-Neo, Proton Savvy, Renault Clio, Renault Twingo, Renault Zoe, SEAT Mii, SEAT Toledo, Skoda Fabia, Skoda Roomster, Smart fortwo, Suzuki Alto, Suzuki Jimny, Suzuki Splash, Suzuki Swift, Suzuki Swift Sport, Suzuki SX4, Toyota Auris, Toyota AYGO, Toyota iQ, Toyota Yaris, Vauxhall Adam, Vauxhall Agila, Vauxhall Corsa, Vauxhall Meriva, Volkswagen Polo, Volkswagen Up.

Cluster 3. Aston Martin DB9, Aston Martin DB9 Volante, Aston Martin V12 Zagato, Aston Martin Vanquish, Aston Martin Vantage, Aston Martin Vantage Roadster, Audi A7 Sportback, Audi A8, Audi R8, Audi R8 V10, Audi RS4 Avant, Bentley Continental, Bentley Continental GTC, Bentley Flying Spur, Bentley Mulsanne, BMW 6 Series, BMW 6 Series Convertible, BMW 6 Series Gran Coupé, BMW 7 Series, BMW M3, BMW M6, Bugatti Veyron, Chevrolet Camaro, Chrysler 300C, Corvette C6, Ferrari 458, Ferrari California, Ferrari F12, Ferrari FF, Infiniti EX, Infiniti G37, Infiniti M, Jaguar F-Type, Jaguar XFR, Jaguar XJ Series, Jaguar XK, Lamborghini Aventador, Lamborghini Gallardo, Lexus IS, Lotus Evora, Lotus Exige S, Maserati GranTurismo, Maserati Quattroporte, McLaren MP4-12C, Mercedes-Benz C63 AMG, Mercedes-Benz CL-Class, Mercedes-Benz CLS-Class, Mercedes-Benz E63 AMG, Mercedes-Benz SL 63, Mercedes-Benz SL-Class, Mercedes-Benz SLS, Morgan Aero, Morgan Road-

ster, Nissan 370Z, Noble M600, Pagani Huayra, Porsche 911, Porsche Boxster, Porsche Panamera, Rolls-Royce Ghost, Rolls-Royce Phantom, Rolls-Royce Phantom Coupé, Vauxhall VXR8, Volkswagen Phaeton.

Cluster 4. Audi Q7, BMW X3, BMW X5, BMW X6, Chevrolet Captiva, Chrysler Grand Voyager, Ford Galaxy, Hyundai i800, Hyundai Santa Fe, Infiniti FX, Jeep Grand Cherokee, Jeep Wrangler, Kia Sorento, Land Rover Defender, Land Rover Discovery 4, Land Rover Range Rover, Land Rover Range Rover Sport, Lexus RX, Mercedes-Benz G-Class, Mercedes-Benz GL-Class, Mercedes-Benz M-Class, Mercedes-Benz R-Class, Mercedes-Benz S-Class, Mitsubishi Shogun, Nissan Pathfinder, Porsche Cayenne, SEAT Alhambra, Ssangyong Rodius, Toyota Land Cruiser, Toyota Land Cruiser V8, Vauxhall Antara, Volkswagen Sharan, Volkswagen Touareg, Volvo XC60, Volvo XC90.

As highlighted in the main article, we analyze this data set via a cluster-oriented approach. However, not all the cars have a perfect assignment to the corresponding cluster. Some of them have a maximum a posteriori probability lower than 0.80, with a moderately high second probability. For instance, the Renault Twizy, Citroen DS3, Nissan Juke, and Volkswagen Golf Plus are assigned to Cluster 1 with probabilities of 0.57, 0.66, 0.71, and 0.77, respectively, and to Cluster 2 with probabilities of 0.34, 0.34, 0.29, and 0.23, respectively. Meanwhile, the Lotus Elise is assigned to Cluster 1 with a probability of 0.67, despite having a 0.32 probability of being associated to Cluster 4. On the other hand, the Suzuki SX4 and Toyota Auris, which belong to Cluster 2 with probabilities 0.66 and 0.74, respectively, would be grouped with compact and mid-size sedans and crossovers (Cluster

1) as a second choice. Finally, the SEAT Alhambra, which belongs to Cluster 4 with a probability of 0.71, would be grouped secondarily with compact and mid-size sedans and crossovers. Cluster 3, on the other hand, has assignment probabilities higher than 0.95.

References

Böhning, D., Dietz, E., Schaub, R., Schlattmann, P., and Lindsay, B. (1994), “The distribution of the likelihood ratio for mixtures of densities from the one-parameter exponential family,” *Annals of the Institute of Statistical Mathematics*, 46, 373–388.

Cappozzo, A., Greselin, F., and Murphy, T. B. (2021), “Robust variable selection for model-based learning in presence of adulteration,” *Computational Statistics & Data Analysis*, 158, 107186.

Cuesta-Albertos, J. A., Gordaliza, A., and Matran, C. (1997), “Trimmed k -means: An attempt to robustify quantizers,” *The Annals of Statistics*, 25, 553–576.

Downey, G. (1996), “Authentication of food and food ingredients by near infrared spectroscopy,” *Journal of Near Infrared Spectroscopy*, 4, 47–61.

Fritz, H., García-Escudero, L. A., and Mayo-Iscar, A. (2012), “tclust: An R package for a trimming approach to cluster analysis,” *Journal of Statistical Software*, 47, 1–26.

— (2013), “A fast algorithm for robust constrained clustering,” *Computational Statistics & Data Analysis*, 61, 124–136.

Ghahramani, Z. and Jordan, M. (1995), “Learning from incomplete data,” Technical Report AI Lab Memo No. 1509, CBCL Paper No. 108, MIT AI Lab.

Goodnight, J. (1979), “A tutorial on the sweep operator,” *The American Statistician*, 33, 149–158.

Grötschel, M., Lovasz, L., and Schrijver, A. (1993), *Geometric Algorithms and Combinatorial Optimization*, 2nd ed., Springer, Berlin.

Hubert, L. and Arabie, P. (1985), “Comparing partitions,” *Journal of Classification*, 2, 193–218.

Knuth, D. (1998), *The Art of Computer Programming. Sorting and Searching*, vol. 3, 2nd ed., Addison-Wesley, Boston.

Little, R. J. A. and Rubin, D. B. (2019), *Statistical Analysis with Missing Data*, 3rd ed., John Wiley & Sons, Hoboken.

Maitra, R. and Melnykov, V. (2010), “Simulating data to study performance of finite mixture modeling and clustering algorithms,” *Journal of Computational and Graphical Statistics*, 19, 354–376.

McLachlan, G. J. and Krishnan, T. (2008), *The EM algorithm and extensions*, 2nd ed., Wiley, Hoboken.

McLachlan, G. J. and Peel, D. (2000), *Finite mixture models*, Wiley, New York.

McNicholas, P. D., Murphy, T. B., McDaid, A. F., and Frost, D. (2010), “Serial and parallel

implementations of model-based clustering via parsimonious gaussian mixture models,” *Computational Statistics & Data Analysis*, 54, 711–723.

Murphy, T. B., Dean, N., and Raftery, A. E. (2010), “Variable selection and updating in model-based discriminant analysis for high dimensional data with food authenticity applications,” *The Annals of Applied Statistics*, 4, 396–421.

Raymaekers, J. and Rousseeuw, P. J. (2023), “The cellwise minimum covariance determinant estimator,” *Journal of the American Statistical Association*, 119, 2610–2621.

Ruwet, C., García-Escudero, L. A., Gordaliza, A., and Mayo-Iscar, A. (2013), “On the breakdown behavior of the TCLUST clustering procedure,” *TEST*, 22, 466–487.